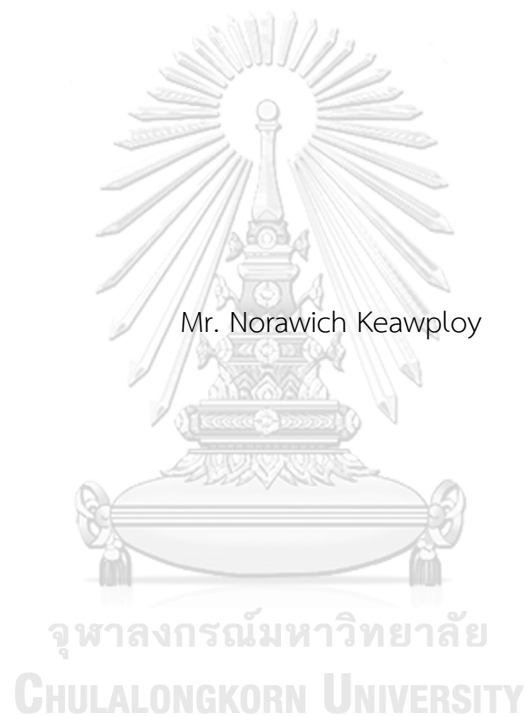Preparation of Ag-CNTs and Ag-Graphene nanocomposite and their combination with MnO$_2$ bath deposition for flexible supercapacitor development.

Mr. Norawich Keawploy

การเตรียม Ag-CNTs และ Ag-Graphene นาโนคอมโพสิต และผสมกับ MnO$_2$ โดยวิธีการใช้อ่างเคมี
สำหรับการพัฒนาตัวเก็บประจุยิ่งยวดแบบโค้งงอได้

นายนรวิชญ์ แก้วพลอย

จุฬาลงกรณ์มหาวิทยาลัย
CHULALONGKORN UNIVERSITY

วิทยานิพนธ์นี้เป็นส่วนหนึ่งของการศึกษาตามหลักสูตรปริญญาวิศวกรรมศาสตรมหาบัณฑิต
สาขาวิชาวิศวกรรมโลหการและวัสดุ ภาควิชาวิศวกรรมโลหการ
คณะวิศวกรรมศาสตร์ จุฬาลงกรณ์มหาวิทยาลัย
ปีการศึกษา 2562

Thesis Title   Preparation of Ag-CNTs and Ag-Graphene
                      nanocomposite and their combination with MnO$_2$ bath
                      deposition for flexible supercapacitor development.
By   Mr. Norawich Keawploy
Field of Study   Metallurgical and Materials Engineering
Thesis Advisor   Assistant Professor PANYAWAT WANGYAO, Ph.D.
Thesis Co Advisor   Jiaqian Qin, Ph.D.

Accepted by the FACULTY OF ENGINEERING, Chulalongkorn University in Partial Fulfillment of the Requirement for the Master of Engineering

.... Dean of the FACULTY OF
ENGINEERING
(Professor SUPOT TEACHAVORASINSKUN, D.Eng.)

THESIS COMMITTEE

.... Chairman
(Professor GOBBOON LOTHONGKUM, Dr.Ing.)

.... Thesis Advisor
(Assistant Professor PANYAWAT WANGYAO, Ph.D.)

.... Thesis Co-Advisor
(Jiaqian Qin, Ph.D.)

.... Examiner
(Associate Professor SEKSAK ASAVAVISITHCHAI, Ph.D.)

.... External Examiner
(Associate Professor Sureerat Polsilapa, Ph.D.)

นรวิชญ์ แก้วพลอย : การเตรียม Ag-CNTs และ Ag-Graphene นาโนคอมโพสิต และ ผสมกับ MnO_2 โดยวิธีการใช้อ่างเคมีสำหรับการพัฒนาตัวเก็บประจุยิ่งยวดแบบโค้งงอได้. (Preparation of Ag-CNTs and Ag-Graphene nanocomposite and their combination with MnO_2 bath deposition for flexible supercapacitor development.) อ.ที่ปรึกษาหลัก : ผศ. ดร.ปัญญวัชร์ วังยาว, อ.ที่ปรึกษาร่วม : ดร. เจียเชียน ฉิน

ปัจจุบันนักวิจัยได้ใช้ความพยายามอย่างมากในการพัฒนาอุปกรณ์จัดเก็บพลังงานที่มีความยืดหยุ่นและน้ำหนัก เบา และจากความก้าวหน้าของอุปกรณ์อิเล็กทรอนิกส์สมัยใหม่ ความต้องการกำลังต่อพื้นที่สูง, สามารถเก็บประจุและปล่อยได้ อย่างว่องไว ซุปเปอร์คาปาซิเตอร์จึงเหมาะสมอย่างยิ่งสำหรับการใช้งานที่ยืดหยุ่นต่างๆ โดยทั่วไปวัสดุนาโนคาร์บอนเช่นท่อนาโน คาร์บอนและแผ่นนาโนกราฟีนจะแสดงประสิทธิภาพของตัวเก็บประจุยิ่งยวดที่ดี รวมไปถึงแมงกานีสไดออกไซด์ (MnO_2) ได้รับ การศึกษาอย่างกว้างขวางสำหรับ pseudocapacitors อันเนื่องมาจากความจุเฉพาะสูง พลังงานสูง และ ความหนาแน่นของ พลังงาน ดังนั้น MnO_2 จึงถูกนำไปใช้เพื่อเพิ่มประสิทธิภาพของตัวเก็บประจุซุปเปอร์คาปาซิเตอร์ของวัสดุคาร์บอน อย่างไรก็ตาม ตัว เก็บประจุยิ่งยวดในปัจจุบันมีขนาดใหญ่มีน้ำหนักมากและไม่ยืดหยุ่นซึ่งไม่เหมาะสำหรับเทคโนโลยีที่สวมใส่ได้ เพื่อเอาชนะความท้า ทายเหล่านี้ ตัวเก็บประจุยิ่งยวดแบบยืดหยุ่น หรือตัวเก็บประจุยิ่งยวดแบบโค้งงอได้ ได้รับการพัฒนาเพื่อตอบสนองอุปกรณ์ อิเล็กทรอนิกส์ที่สวมใส่ได้ วัสดุผ้าฝ้ายได้รับการพิจารณาอย่างกว้างขวางสำหรับพื้นผิวที่มีความยืดหยุ่นเนื่องจากเส้นใยธรรมชาติ ราคาไม่แพงและมีน้ำหนักเบา ในงานนี้ผ้าฝ้ายนำไฟฟ้าได้รับการเตรียมด้วยวิธีการพิมพ์สกรีนโดยใช้หมึกที่พัฒนาขึ้น ผ้าฝ้ายนำไฟฟ้า ที่เตรียมไว้มีความต้านทานต่ำน้อยกว่า 15 โอห์ม/ซม. นอกจากนี้อิเล็กโทรดของตัวเก็บประจุแบบยิ่งยวดยังถูกประดิษฐ์ขึ้นได้โดยการ ผสมวัสดุคาร์บอน (CNT และกราฟีน) ลงในหมึกที่พัฒนาขึ้น ในปริมาณของคาร์บอนที่แตกต่างกันนี้ ขั้วไฟฟ้า CNT แสดง ประสิทธิภาพทางเคมีไฟฟ้าที่เหนือกว่า (78.49 mF / cm^2 ที่ 0.1 mA / cm^2) เพื่อเพิ่มความจุเฉพาะเพิ่มเติม MnO_2 ถูกเคลือบบน อิเล็กโทรดโดยการสะสมของสารเคมี (CBD) โดยใช้ด่างทับทิมและสารละลายกรดซัลฟิวริก ได้ความจุจำเพาะที่สูงถึง 741.83 mF / cm2 ที่ 0.1 mA / cm^2 ในที่สุดอุปกรณ์ซุปเปอร์คาปาซิเตอร์แบบยืดหยุ่นก็ถูกประดิษฐ์ขึ้นมาได้สำเร็จซึ่งแสดงให้เห็นถึงความจุ เฉพาะเจาะจงสูงที่ 677.12 mF / cm^2 ที่ 0.0125 mA / cm^2 สำหรับขั้วไฟฟ้า CNT อุปกรณ์ที่มีความยืดหยุ่นยังแสดงให้เห็นถึง ประสิทธิภาพอัตราที่ยอดเยี่ยมและความเสถียรของวงจรด้วยการกักเก็บความจุ 80% เป็นเวลา 3000 รอบซึ่งแสดงให้เห็นว่า สามารถผลิตอุปกรณ์จัดเก็บพลังงานแบบยืดหยุ่นได้

สาขาวิชา	วิศวกรรมโลหการและวัสดุ	ลายมือชื่อนิสิต ....
ปีการศึกษา	2562	ลายมือชื่อ อ.ที่ปรึกษาหลัก ....
		ลายมือชื่อ อ.ที่ปรึกษาร่วม ....

5970442421 : MAJOR METALLURGICAL AND MATERIALS ENGINEERING

KEYWORD: conductive cotton; flexible supercapacitor; wearable electronics; energy storage, composite

Norawich Keawploy : Preparation of Ag-CNTs and Ag-Graphene nanocomposite and their combination with MnO_2 bath deposition for flexible supercapacitor development.. Advisor: Asst. Prof. PANYAWAT WANGYAO, Ph.D. Co-advisor: Jiaqian Qin, Ph.D.

Nowadays, researchers have made great efforts on the development of flexible and light weight energy storage devices for their practical applications and the advancement of modern electronic devices. Owing to the promising feathers of high specific power, high rate capability, and long-term cycling life, the supercapacitors (SCs) are considered as highly suitable for various flexible applications. In general, the carbon-based nanomaterials such as carbon nanotubes and graphene nanosheets, exhibit good supercapacitor performance. Manganese dioxide (MnO_2) are widely studied for pseudocapacitors owing to their high specific capacitance, high power, and energy density. Thus, MnO_2 was applied to increase the supercapacitor performance of carbon materials. However, most of the reported SCs are bulk, heavy, and non-flexible, which are not suitable for wearable energy technology. To overcome these challenges, flexible supercapacitors (FSCs) are developed to meet the wearable electronics. The cotton cloth materials are widely considered for flexible substrates due to inexpensive natural fiber, highly hydrophilic and light weight. In this work, the conductive cotton was successfully prepared by the screen-printing method using the developed ink. The designed textile ink and silver powder mixture demonstrates an outstanding conductivity. The prepared conductive cotton reached a low resistance of less than 15 ohm/cm^2. Furthermore, the supercapacitor electrodes were also fabricated by mixing the active materials (CNT, and graphene) into the developed ink. Among these different carbon electrodes, the CNT electrodes show superior electrochemical performance (78.49 mF/cm^2 at 0.1 mA/cm^2). To further enhance the specific capacitance, the MnO_2 was coated on the electrodes by chemical bath deposition (CBD) using potassium permanganate and sulfuric acid solution. The specific capacitance of as high as 741.83 mF/cm^2 at 0.1 mA/cm^2 was achieved. Finally, the flexible supercapacitor device was also successfully fabricated, which exhibited a high specific areal capacitance of 677.12 mF/cm^2 at 0.0125 mA/cm^2 for CNT electrodes. The flexible device also shows excellent rate performance and cyclic stability with capacitance retention of 80% for 3000 cycles, demonstrating that advanced flexible energy storage devices can be achieved.

Field of Study:	Metallurgical and Materials Engineering	Student's Signature ....
Academic Year:	2019	Advisor's Signature ....
		Co-advisor's Signature ....

ACKNOWLEDGEMENTS

TABLE OF CONTENTS

จุฬาลงกรณ์มหาวิทยาลัย

CHULALONGKORN UNIVERSITY

LIST OF TABLES

จุฬาลงกรณ์มหาวิทยาลัย
CHULALONGKORN UNIVERSITY

LIST OF FIGURES

Chapter 1

Introduction

1.1 Energy storage and Flexible supercapacitor

The leap in the development of smart technology leads to an increase in energy demand. Supercapacitors and battery are store chemical energy that is converted into electricity to operate mobile phones and other devices.

Supercapacitor, also named electrochemical capacitors or ultracapacitors, are electrical devices that can accommodate and store

Electrochemical capacitors, also named supercapacitors or ultracapacitors, are electrical devices that can store and accommodate certain amounts of energy. Supercapacitor is used in devices where there is a need to store and release huge amounts of energy in a short time. [1].

Supercapacitor (SCs) is a type of capacitor that can store a large amount of energy, typically 10 to 100 times more energy density compared to conventional capacitors. It is preferred over batteries owing to its faster charging and faster delivery of electricity [2, 3]. SCs can be divided into three basic categories according to the energy storage mechanism [1]. The first type is Electrical double layer capacitors (EDLCs). The EDLCs use electrostatic interaction to accumulate energy in the Helmholz double layers on the interface between the electrolyte and the surface of electrodes.

Electrical double layer capacitors (EDLCs) arises from the potential-dependence of the surface energy stored electrostatically at the interface of the capacitor electrodes. In this type, there is no electron exchange and no redox reaction. The key point to obtain an extremely high capacity is the Helmholtz layer thickness and the large surface area of the electrodes. EDLCs possess god cycle

stability and durability [2]. The materials of this type are used various carbon materials such as activated carbon, carbon nanotube (CNTs) and graphene [3]. The second category is called pseudocapacitor or faradic supercapacitors. By operation principle, pseudocapacitance in a phenomenon where electrons transfer and occur redox reaction. The pseudocapacitor arises at the electrode surfaces, where faradaic reactions begin, and the reactions involve the passage of energy across the double layer. During charge and discharge, pseudocapacitor generates a redox reaction and energy transfer between electrode and electrolyte. The disadvantage of this system is the electrodes are stressed, and degrade faster during charging and discharging, compared to EDLC. It affects to increasing the resistance of supercapacitors. Pseudocapacitor made by pseudocapacitive materials such as ruthenium oxide (RuO_2) and manganese dioxide (MnO_2). The cycle life and stability are lower than EDLCs. The third is called the hybrid supercapacitors. It is the newest type of supercapacitor. The hybrid supercapacitor combines both EDLCs and pseudocapacitors advantages. The advantage is higher volumetric and gravimetric energy density with the capability to provide high currents. Due to the faradaic reaction that occurs on the negative electrode, which is typically made from pseudocapacitive electrode materials. The positive electrode is typically made from activated carbon that stores electrostatic energy in the double layer on the electrode surface. The hybrid supercapacitors can deliver high currents. Presently, they are not commercially available in the market and are still investigated in laboratory conditions.

Supercapacitors currently fill the gap between batteries and conventional capacitors (Figure 1-2). They store thousands of times more charge than the latter because a much larger surface area (1,000 – 2,000 m^2/g) is available for charge storage in EDLC. However, they are a lower energy density than those of batters. If a supercapacitor is used in an electric vehicle, the specific energy displays how far one can go on a single charge, the specific power shows how fast one can go. [2].

Table 1 Summarization and comparison of important attributes of energy storage devices [1].

Attribute	Supercapacitor (SC)		Lithium-ion battery
	EDLC	Pseudo	
Charge time [s]	1-10	1-10	600
Cycle life	1 M	0.1 M	500
Cell Voltage [V]	2.7	2.3-2.8	3.6
Specific energy [Wh/kg]	3-5	10	250
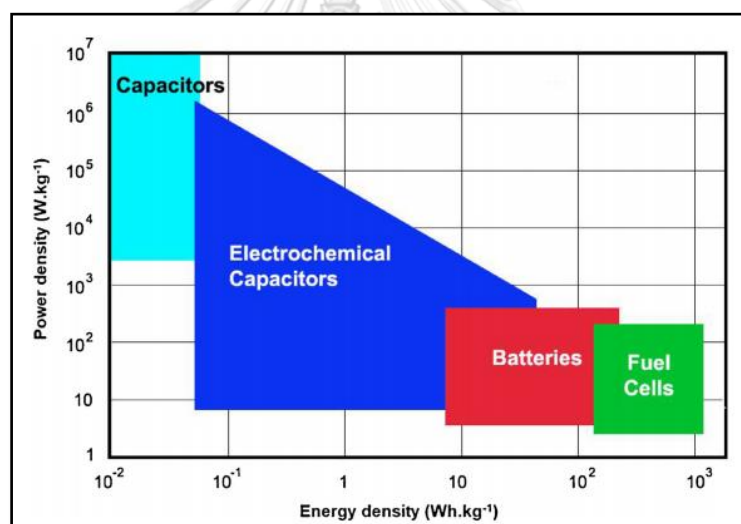
Figure 1 Ragone chart: Power density as a function of energy density for various energy storage devices [1].

In the future, the electronic devices will be twistable and deformable, thereby wearable applications would be impossible to achieve by using the hard and rigid electronics device. Energy storage devices with flexibility, lightweight and safety may be in large demand. With the rapid development of portable and wearable

electronics in recent years, the fabrication of flexible energy storage devices has become an emerging field [4].
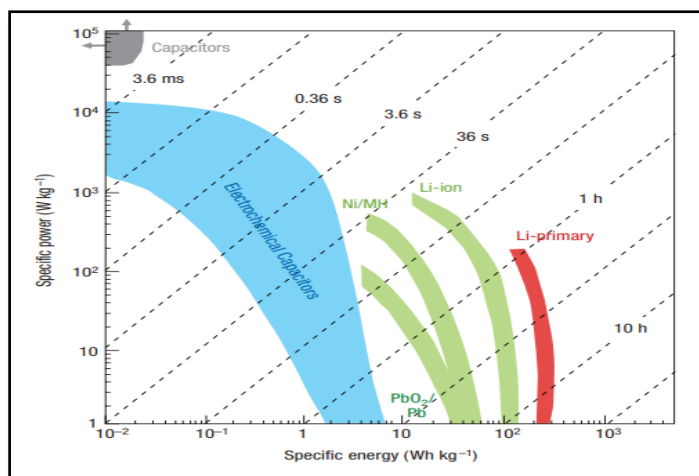
Figure 2 Ragone plot for various electrical energy storage devices [2].

Flexible supercapacitors (FSCs) can be divided into three groups: fiber-like FSCs; paper-like FSCs; and three-dimensional (3D) porous FSCs. Based on the above classification method, the mechanical properties and electrochemical performances of each type of flexible supercapacitors are parsed [5].
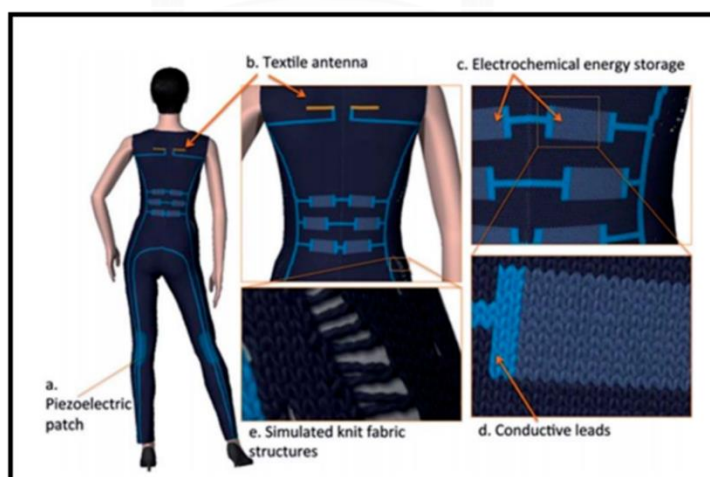
Figure 3 Illustration of Flexible supercapacitor device fabricated in wearable clothes [5].

A smart is an electronic gadget that can connect and interact with other smart devices (Figure 3). Smart devices are interactive electronic gadgets which comprehend simple commands that are imparted by users. They also support activities in daily life. Smart phones, tablets, phablets, smartwatches, smart glasses are the most used smart devices as personal electronics. Smart devices are defined by their performances to connect to a network to share and interact remotely.

The wearable device is a small electronic device that can be worn on our bodies. It has a self-working style, without having to rely on another device or can also work with other devices. The popular wearable devices are the smartwatch and wristbands. These devices are equipped with sensors, which can count walking/running steps, heart rate, sleep condition analysis, calculate calorie burning, etc [6].

This research will aim to prepare the conductive material (carbon nanotube, silver powder, graphene nanosheet) in the block screen color. To further enhance the supercapacitor performance, MnO_2 was introduced by chemical bath deposition to modify the conductive cotton electrode. The phase composition, morphology, electrochemical performance, specific capacitance, power density and cycle stability will be characterized and tested.

1.2 Objectives

1. To prepare Ag-CNTs, Ag-graphene and Ag-CNTs-graphene nanocomposites on cotton cloth.

2 To study the effect of MnO_2 on the supercapacitor performance of Ag-CNTs/graphene nanocomposite.

3. To develop & fabricate flexible supercapacitor on the cotton cloth.

1.3 Scopes

Set 1:

1. Preparation of solutions for conductive layers on cotton cloth with the composition below:

1.1 Mixing Ag and CNTs powders by volume following fractions: Ag:CNTs 1:0 ,0.8:0.2 and 0.6:0.4, respectively. Then mixing with textile ink color.

1.2 Mixing Ag and Graphene powders by volume following fractions: Ag: Graphene, 1:0, 0.8:0.2 and 0.6:0.4, respectively. Then mixing with textile ink color.

1.3 Mixing Ag, Graphene and CNTs powders by volume following fractions: Ag:Graphene:CNTs , 0.6:0.2:0.2 ,0.6:0.1:0.3 ,0.6:0.3:0.1 and 0.8:0.1:0.1, respectively. Then mixing with textile ink color.

2. Casting these obtained slurry on cotton cloths to fabricate the conductive cotton as current collector and electrode.

2.1 Before and after painted cotton cloths will be characterized by SEM.

2.2 Painted cotton will be tested for electrochemical performance by the galvanostatic method in 6 M KOH.

2.3 Immersing these painted cotton cloths with the PVA-KOH electrolyte.

2.4 The flexible supercapacitor will be assembled by 2 pieces of painted cotton cloths with PVA-KOH gel electrolyte.

2.5 The specific capacitance, power density, energy density will be performed and evaluated.

Set 2:

1. Preparation of slurries for conductive layers on cotton cloth with selected optimum conditions (the highest specific capacitance) from each group of set 1.

2. Painting these obtained slurries on cotton cloths to fabricate the current collector and electrode.

3. Coating MnO_2 on these painted cotton cloths by bath deposition in 1x4 cm^2 area which consists of 2 groups as follows

3.1 Solution A: 0.03M $KMnO_4$ + 0.02 M Citric (Time 15,30,45,60 min)

3.2 Solution B: 0.03M $KMnO_4$ + 0.06 M H_2SO_4 (Time 15,30,45,60 min)

4. The phase composition and morphology will be characterized by SEM and XRD.

5. Painted cotton will be tested for electrochemical performance by the galvanostatic method in 6 M KOH.

6. Immersing these coated cotton cloths with PVA-KOH to form gel electrolytes on these cloths.

7. Assembling 2 pieces of coated cotton cloths with gel electrolyte to fabricate flexible supercapacitor.

8. The specific capacitance, power density and energy density will be performed and evaluated

จุฬาลงกรณ์มหาวิทยาลัย

CHULALONGKORN UNIVERSITY

Chapter 2

Literature review

2.1 Wearable electronics

Wearable technologies are smart electronic devices that can be incorporated into the costume or cover on the skin as accessories or implants (Figure 4) [7].
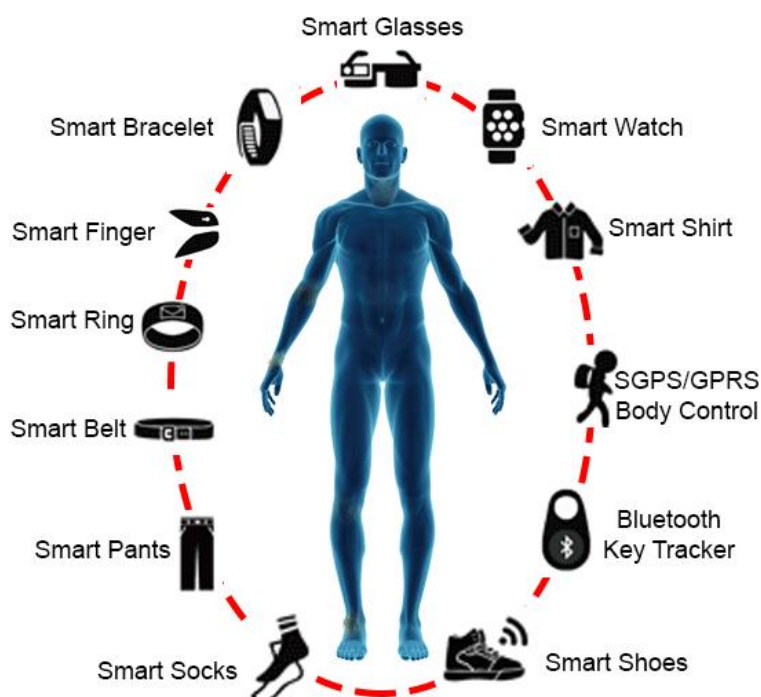
Figure 4 Illustrating different types of wearable electronics [8].

The advantage of wearable technology are small, worn discreetly in any environment, personal data can be collected into communication networks and facilitating remote monitor [6]. It can be used for applications, such as fitness monitor, sports performance and health care (Heart rate, calories burned, steps walked, blood pressure) [8, 9]. Wearable energy storage systems have many applications, such as power source for medical bio monitor devices or implants, military equipment for soldier , safety and construction gear like illuminated vests [10]. It is believed that these electronics will bring change to the human lifestyle [11].

2.2 Supercapacitors

Supercapacitors have promising energy storage use in portable electronic devices, such as mobile phones, laptops, wearable devices, Hybrid Electric Vehicles (HEV), Electric Vehicles (EV), etc. Many researchers are study for flexible, lightweight and environmentally friendly devices. The supercapacitor is the gap between batteries and conventional capacitors by providing higher power density with longer cycle life batteries and higher energy density than conventional capacitors, the three main of electrochemical energy storage technology that used in wearable devices (ranging from high power to high energy respectively) are batteries, pseudocapacitors and electrical double-layer capacitors (EDLC). Both the pseudocapacitor and electric double-layer capacitor are normally called "supercapacitor" [10]. Supercapacitors are consisted of two current collectors, two electrodes (active materials, e.g., MnO_2 and carbon), an electrolyte (KOH), and a separator membrane. (Figure 5)
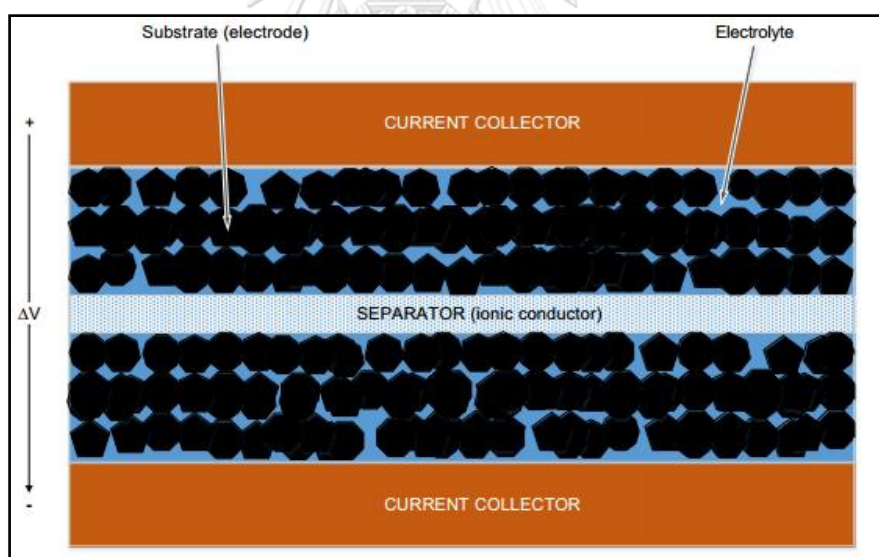
Figure 5 Schematic diagram of the supercapacitor [12].

In general, supercapacitors are common in the industry in three categories, which are electrochemical pseudocapacity (PC), electrical double layer capacitors (EDLCs) or electrostatic and hybrid supercapacitor (HSC). EDLCs receive more attention due to their properties of the rapid charge-discharge process, high power

density, long and excellent cycle ability [13, 14]. Furthermore, EDLC energy storage undergoes charge accumulation by electrostatic interaction of charge separation at the interface between the conductive electrode surface and the electrolyte (Helmholtz double layers). The double-layer capacitance arises from the potential dependence of electrostatically stored surface energy on the interface of capacitor electrodes. Such supercapacitors have neither electron exchange nor redox (non-faradaic) reaction. The main criteria in obtaining outstanding high capacity are due to the development of a large electrode surface area which depends on the thickness of the Helmholtz layer. The characteristic of EDLC supercapacitors are carbon-based materials, such as carbon nanotubes (CNTs), activated carbon (AC) and graphene nanosheets due to the large specific surface area (SSA), low cost, high abundance material and facile production [15-18]. Figure 6 shows basic schematics for an (a) all carbon EDLC, (b) pseudocapacitors and (c) lithium-ion battery.
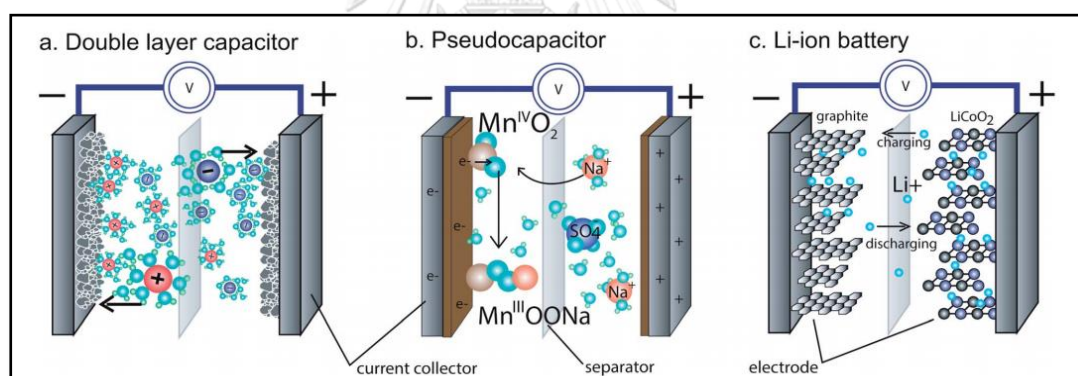
Figure 6 Basic schematics for an (a) all carbon EDLC, (b) pseudocapacitor and (c) lithium ion battery [10]

2.2.1 Mechanism of Electric double layer.
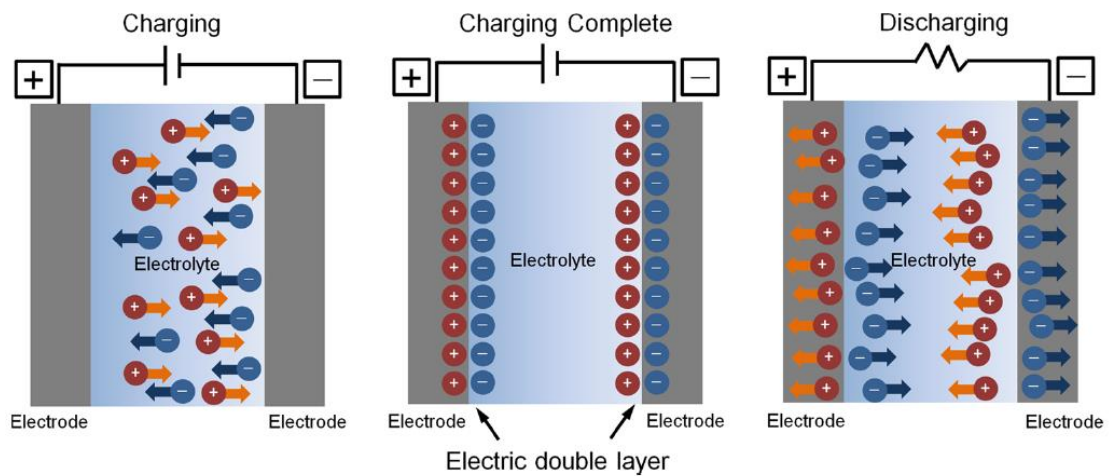
Figure 7 Charge distribution characteristics during charging (left) when fully charged (neutral) and when discharge (right) [19].

Figure 7 When giving the voltage or current to both electrodes, such as when connecting supercapacitors to batteries, the positive charge inside the electrolyte dissolution is attracted to the cathode of the supercapacitor. A negative charge in the solution will go to the anode. The use of carbon with the high surface area and porous volume increases the capacitance because the charge of the electrolyte solution can be inserted into the pores. There are many theoretical models between solid-liquid interfaces, i.e., three models are as follows.

Helmholtz model is the simplest estimation for modeling the spatial distribution of charges at the interface of double layer. The solid electronic surface charge is neutralized by opposite sign counterions. The distance, d, is from the surface to the center of the counterions. However, the Helmholtz theoretical does not adequately explain all the features since it considers rigid layers counterbalancing the opposite charges, Figure 8 (IHP = Internal Helmholtz double layer, OHP = outer Helmholtz double layer) [12].

Gouy–Chapman (diffuse model), Gouy suggested that the opposite ionic charge at the same number presents in a liquid around a charged solid, but the ions

are not attached to the surface. They tend to diffuse into the liquid phase until the counter potential set up by their departure restricts this tendency. The thickness of the diffuse layer is partially affected by the kinetic energy of the ions in the solution. Gouy and Chapman developed theories of this diffuse layer in which the ion concentration near a charged surface follows the Boltzmann distribution. However, this model is incapable of highly charged double layers. In the experiment, the measured thickness of double layers is greater than that obtained by calculation.

Stern modified the Gouy–Chapman model by making a better approach to reality than the Helmholtz model but still has limited applications in quantitative. It is assumed that the ions behave as point charges, they can access the surface with no physical limits, which is not true. Therefore, Stern modified the Gouy–Chapman model. His theory states that ions have a finite size, so cannot approach closer to the surface. The first ions of the Gouy-Chapman Diffuse Double Layer are not at the surface. They are at some distance δ away from the surface, but the Stern model assumes that there can be specifically surface-adsorbed ions in-plane δ, which is known as the Stern layer. The compact layer is formed when ions are strongly adsorbed by the electrode. In the compact layer, there are both specifically adsorbed ions (forming the inner Helmholtz plane), and nonspecifically adsorbed counter-ions (forming the outer Helmholtz plane).
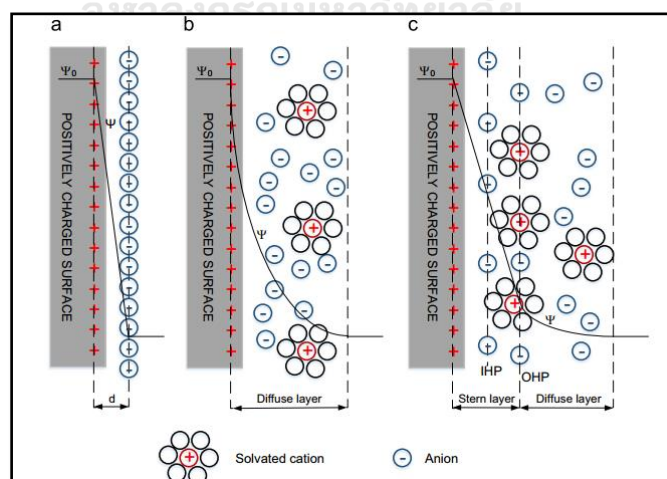
Figure 8 EDL models, (a) Helmholtz model, (b) Gouy–Chapman model, and (c) Stern model [12].

2.2.2. Mechanism of Pseudocapacitors.

Pseudocapacitors store energy through a faradaic process that involves fast and reversible redox reactions occurring at or near the electrode surface. As shown in Figure. 9b, when started to apply potential, the electrode materials occur reversible redox reactions, generate charges and resulting in current passing through the supercapacitor cell. Since the capacitance depends on the faradaic charges generated on the electrode surface, it is extremely important to use pseudo-capacitive materials with high charge generation and storage ability in the short term. The most widely explored pseudo-capacity electrode materials are including conductive polymers such as polyaniline, polypyrrole, and polythiophene) and transition metal oxides or hydroxides (RuO_2, MnO_2, Co_3O_4, NiO, CuO, Fe_2O_3, $Ni(OH)_2$, and $Co(OH)_2$. Comparing EDLCs and pseudocapacitors can receive higher energy density as they can provide a variety of oxidation states for efficient redox charge transfer which could satisfy the needs of high-energy SCs. The challenges associated with pseudocapacitors are rate capability and cycling stability. [20]
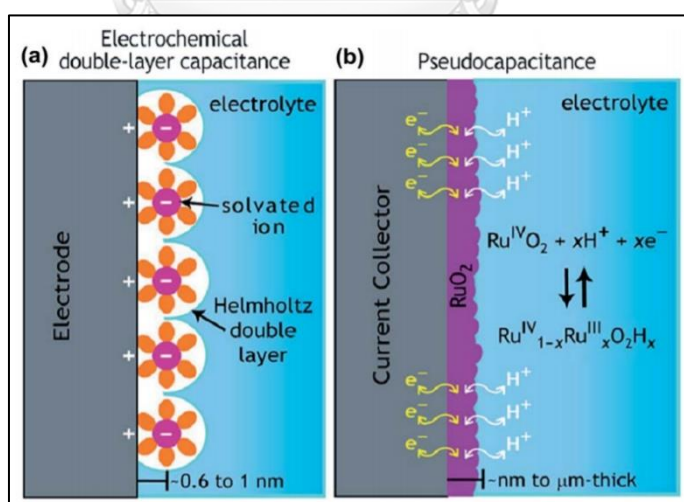
Figure 9 Schematic illustration of two different charge storage mechanisms via (a) electrochemical double-layer capacitance (EDLC) and (b) redox reaction based pseudocapacitance [20].

2.3 Flexible supercapacitor

In Flexible supercapacitor, cheap, flexible, lightweight, wearable power conversion and storage devices are required in all electronic applications. However, conventional charging storage devices such as battery without heavy or bulky, can usually not provide the power needed [12]. To support the development of these electronics, energy-storage devices with the result of good deeds of outstanding electrochemical performance and good flexibility are highly required. Supercapacitors and batteries are perfect devices for energy storage that can satisfy the demand for flexible and wearable electronics for storage. However, the rigid and bulky of commercially available supercapacitor and battery systems are difficult to incorporate into integrated and complex devices [11]. The substrates of flexible supercapacitors are made by Plastic fiber, Carbon fiber and Cotton

All these electronic applications require cheap, flexible, lightweight, wearable power conversion and storage devices. However, conventional charge storage devices, such as batteries, usually cannot provide the needed power without becoming too heavy or bulky To support the development of these electronics, energy-storage devices with the merits of good electrochemical performance and outstanding flexibility are highly required. Supercapacitors and batteries are ideal energy-storage devices that can well meet the energy demand for flexible and wearable electronics. However, current commercially available supercapacitor and battery systems are still rigid and bulky; it is difficult to incorporate them into integrated and complex devices There are many substrates for making flexible supercapacitors such as Plastic fiber, Carbon fiber and Cotton.

2.3.1 Plastic fiber

Plastic fibers support flexible supercapacitors and are inexpensive, flexible and mechanically powerful. Plastic fibers are simple to use as fibrous structural supports in fiber-like FEs [5]. Through a dip-coating method, Yongping Fu [21] coated the surface of a plastic fiber with commercial pen ink. The pen ink component is

shown in Figure10a. The specific surface area is 27.4 m2. The prepared pen ink/plastic fiber electrodes were then assembled into a supercapacitor with 19.5 mF/cm^2 (equal to 0.504 mF/cm), 2.7 mWh/cm^2 and 9,070 mW/cm^2 respectively in capacitance, energy density and power density. The flexible supercapacitor had a very long operation life and excellent flexibility; there was no capacity decay after 15,000 cycles in cyclic voltammetry (CV) tests [21]. The symmetrical triangular curves and the relatively low IR (current time resistance) decrease display excellent capacitive behavior in Figure 11[21].
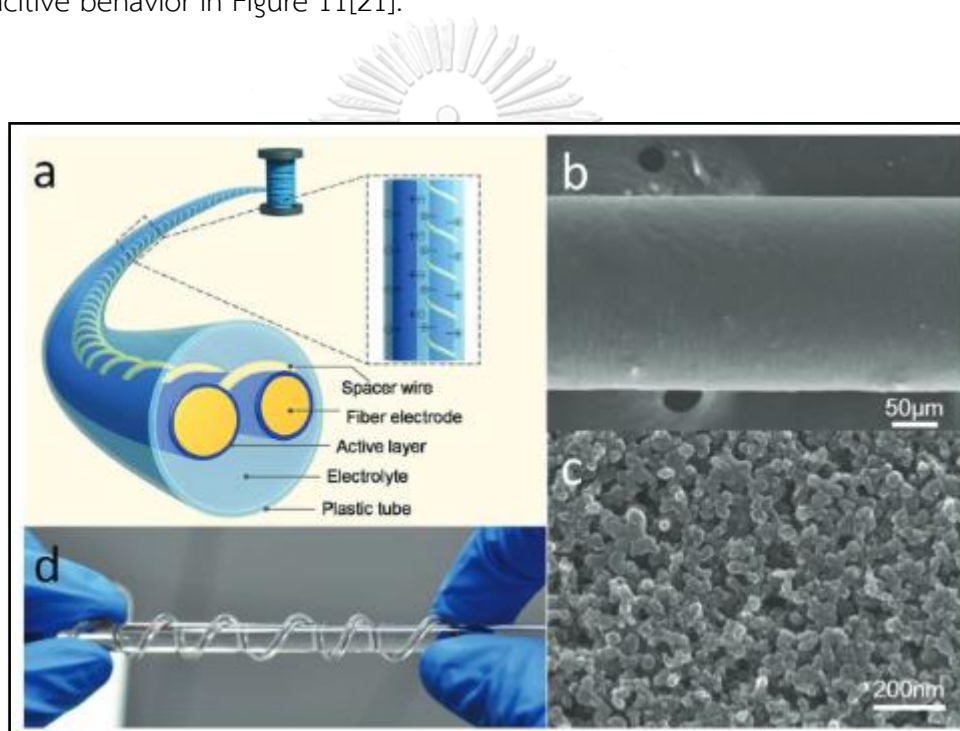
Figure 10 (a) Schematic diagram of the flexible supercapacitor. (b) SEM image of the plastic fiber electrode coated with pen ink film. (c) SEM image of ink nanoparticles at high magnification, with a particle size of around 20 nm. (d) Photograph of a flexible FSC packaged [21].
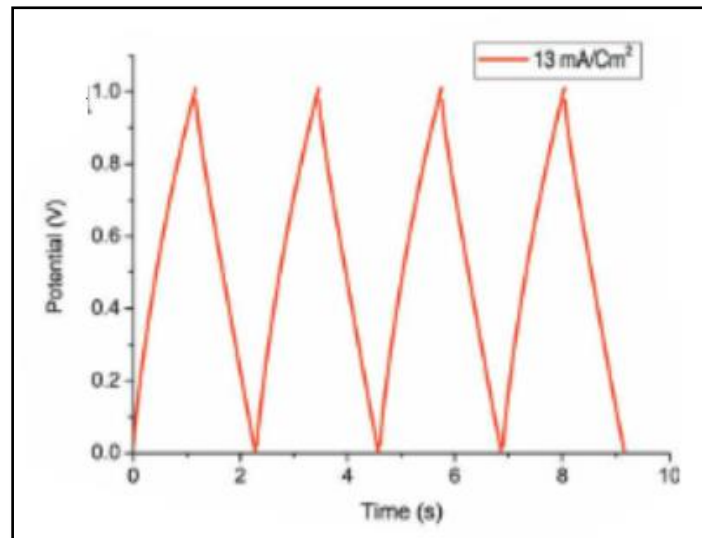
Figure 11 Galvanostatic charge/discharge curves for the FSC at high current density (13 mA/cm^2) [21].

2.3.2 Carbon fiber

Carbon fiber (CF) flexible supercapacitor is a highly conductive, mechanically strong chemical [5]. Viet Thong Le, et al. [22] prepared carbon nanotube with carbon fiber bundle by spraying CNTs (solution) on carbon fiber (Figure 12a). The flexible supercapacitor demonstrates good electrochemical performance (Figure 12b.). The specific capacitance was 6.3 mF/cm and 86.8 mF/cm^2, respectively, and energy density was measured to be 9.8 mWh/cm^2 (0.7 mWh/cm) at power density of 189.4 mW/cm^2 (13.7 mW/cm). The carbon fiber is suggested as a promising application for future of supercapacitor in wearable energy storage. Although, carbon firber are also expensive.
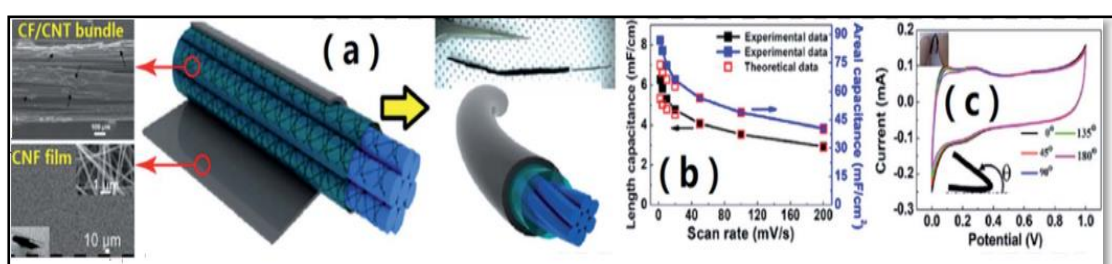
Figure 12 a) CF bundle based fiber-like FEs and corresponding FSCs. Preparation method of coaxial FSC with an inner electrode of a CF/CNT bundle and an outer electrode of a CNF film. b) Capacitance vs. scan rate curves. c) Bending test [22].

2.3.3 Cotton

Up to now, various flexible energy-storage systems with excellent electrochemical performances and suitable mechanical durability are fabricated on flexible substrates such as metal wires, metal sheets, papers, fibers, textiles, and polymer thin films, have been improved compatibility with wearable applications. [10]. Cotton fabrics are widely used as textile materials due to their high durability, cheapness, easy processing, and excellent mechanical properties [23]. The properties of cotton cloth are flexible and porous fabric which is made by weaving natural cotton fibers [11].

2.4 Conductive cotton

Conductive textiles were made from the coating of conductive polymers, metal and metal oxide nanoparticles such as Cu^{2+}, Ni^{2+}, Ag^{2+} and carbonaceous materials such as carbon nanoparticles, carbon nanotubes (CNTs) and graphene oxide (GO).

The electrically conductive superhydrophobic textiles can be fabricated by using atomic layer deposition, dip-coating, knitting, layer by layer assembly, electroless deposition (ELD), in-situ deposition and direct coating of active materials on fiber or yarn or textile substrates, electrically conductive superhydrophobic textiles can be produced using a commonly used direct-coating process applicable to different active materials as well as conducting agents. In situ growth of active materials onto cotton substrates. Active materials are synthesized in situ on the surfaces of the desired substrate in this approach [9].

2.4.1 Electroless

Table 2 Experimental Procedures [24].

Item	Concentration of each solution	Application condition
Precleaning	2% nonionic detergent	20 min, 40 ± 1 $^{\circ}$C
Sensitization	$SnCl_2 \cdot 2\ H_2O$ and HCl	10 min, 25 ± 1 $^{\circ}$C
Plating	$AgNO_3$, NaOH, NH_4OH	50 min, 10 ± 1 $^{\circ}$C
	Glucose	50 min, 10 ± 1 $^{\circ}$C
Posttreatment	DI water	20 min, 40 ± 1 $^{\circ}$C
	Heat	1 min, 150 ± 1 $^{\circ}$C
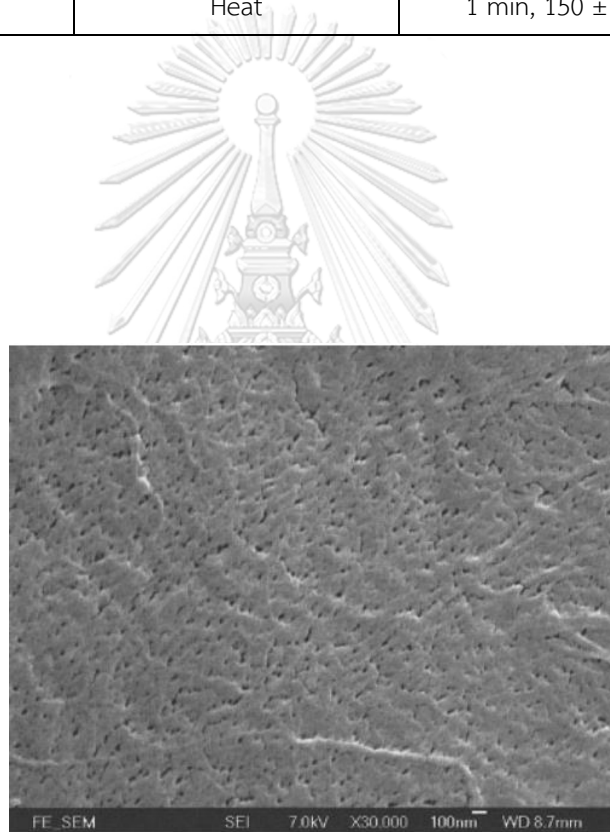
Figure 13 SEM image of the silver-plated cotton fiber.

S. Q. Jiang [24] studied the operation and final properties of the chemical silver plating of cotton by using 4 processes. The experimental procedures are summarized in Table 2. Figure 13 shows the surface appearance before and after silver-plating on cotton cloth and the average resistance was 504 ohms.

2.4.2 Dipping and drying

Conductive cotton fabric was prepared via a dip-and-dry method by coating single-wall carbon nanotubes (CNTs) on a knitted cotton fabric surface [25]. Figure 14 shows a dip-and-dry method for the CNT-cotton fabric (CCF). Neat, elastic fabrics of knitted cotton were soaked in ethanol for 30 minutes and then thoroughly washed with deionized water. A stable CNT suspension was obtained by dispersing the CNTs in water followed by 15 min sonication at room temperature. The cotton fabric (4 cm × 4 cm) was soaked in various concentrations of CNT suspension (0.025, 0.050, 0.075, 0.10 wt.%) and sonicated for 20 minutes at room temperature. Then, the cotton was dried at 40 °C. The color of the fabric changed from white to black after the adsorption of CNTs. Different cycles of "dip-and-dry" were performed to obtain the CCF
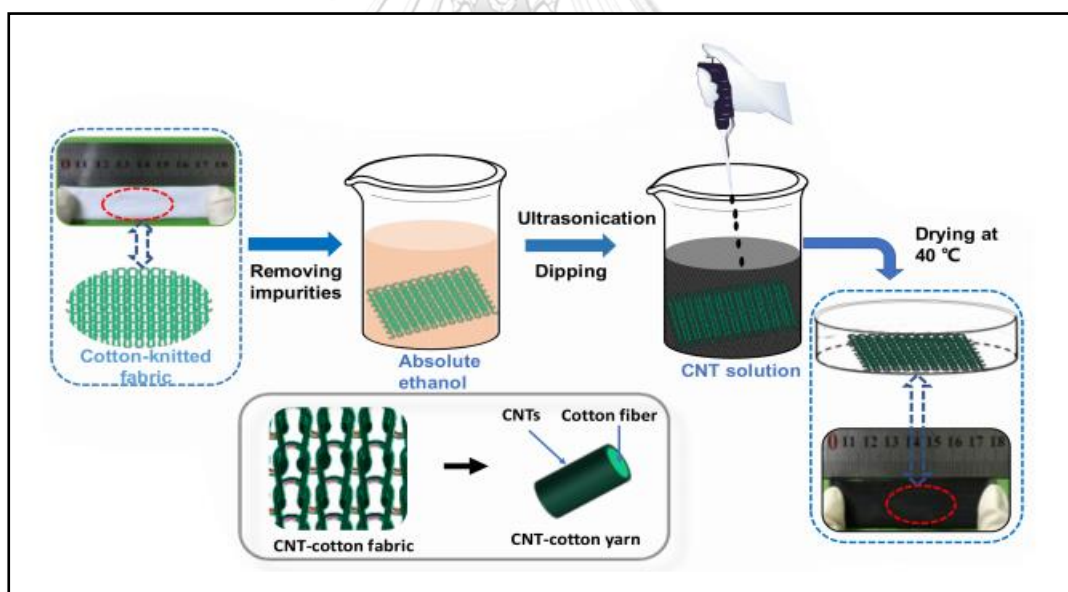
Figure 14 Preparation process of CNT-cotton fabrics. [25]
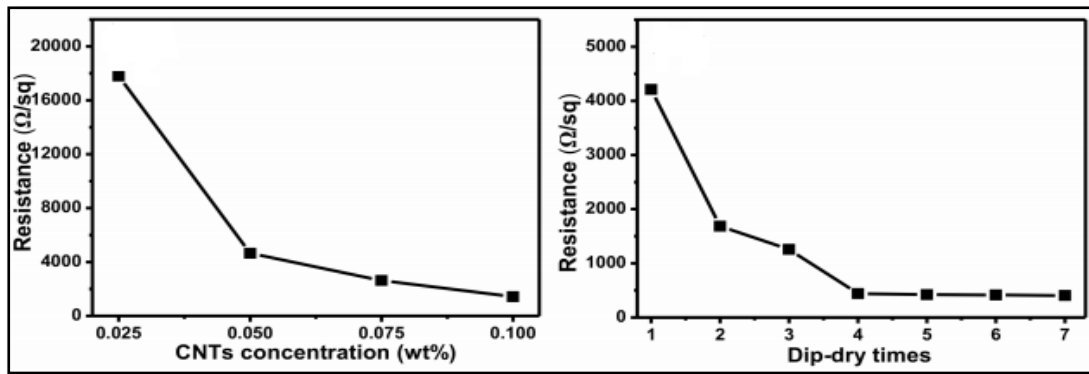
Figure 15 (Left) electrical resistivity of CNT-cotton fabrics corresponding to different CNT concentrations (one dip-dry cycle); and (Right) different numbers of dip-dry cycles (0.05 wt. % of CNT concentration) [25].

The surface resistance decreased significantly when the carbon nanotubes concentration increased from 0.025 to 0.1 wt. %. The average surface electrical resistance The average surface electrical resistance of CCF reached 1,435 ohms/sq. when the CNT concentration was 0.1 wt. %. In addition to CNT concentration, the number of dip-dry cycles has a remarkable effect on the electrical resistance of CCF (Figure 15 Left) and the resistance of CCF was 4,211 ohms/sq. after the first dip-dry cycle. The resistance of CCF decreased greatly with an increasing number of dip-dry cycles and decreased to 439 ohms/sq after four dip-dry cycles (Figure 15 Right) [25].

Yi Cui's group at Stanford University [26] has their work focused on the "dipping and drying" process for coating single-walled carbon nanotubes (SWCNTs) on cotton fabric (Figure 16a-b). Hu et al. fabricated SWCNT-fabrics into stacked electrode sandwiches with a separator and used LiPF6 electrolyte. The SWCNT-fabrics showed high capacitances of 480 mF/cm2 for devices tested at 1 mA/cm2 and 120 F/g with mass loading as 8 mg/cm2. However, this paper had a few unanswered concerns, mainly toxicity, (e.g., LiPF6 electrolyte) that were identified by the electrochemical community.
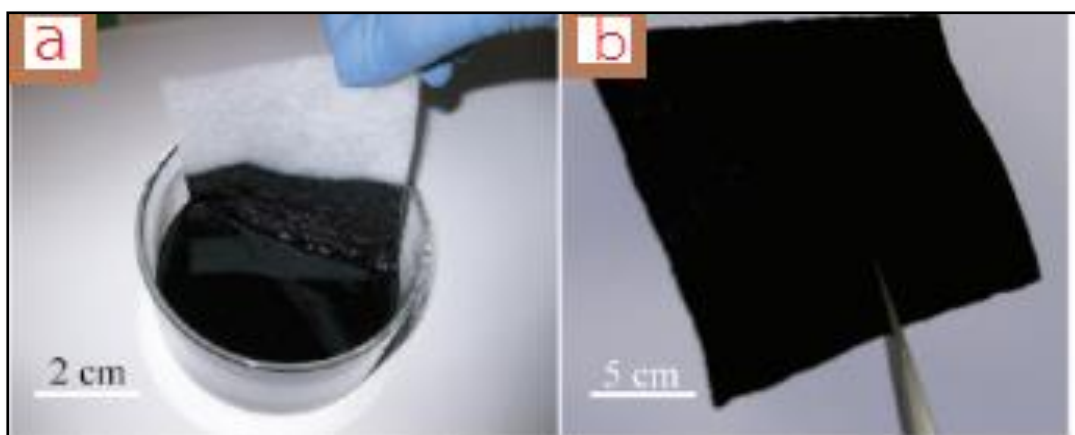
Figure 16 (a) Conductive textiles are fabricated by dipping textiles into an aqueous SWNT ink followed by drying in an oven at 120 °C for 10 min. (b) textile conductor based on a fabric sheet with cotton and R = of 4 ohms/sq [26].
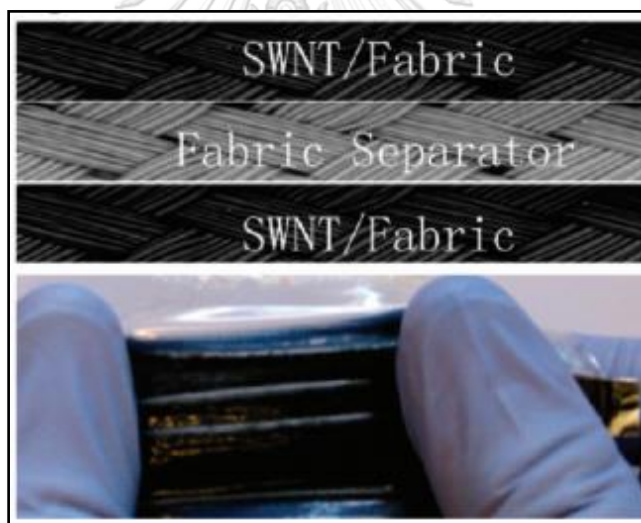
Figure 17 The schematic of flexible supercapacitor with SWNT/fabric as electrodes [26].

2.4.3 Brush-coating and drying

Wen-wen Lui [11] prepared easily processed and the flexible electrode via brush-coating and drying method (Figure 18). The cotton cloth is substate and stable graphene oxide (GO) suspension as the ink. The supercapacitor demonstrates of 81.7 F/g in 6M KOH electrolyte. The Graphene oxide was painted onto the cotton cloth. Subsequently, the cotton absorbed with GO ink was subjected to the drying process

for the removal of water by putting it in an oven at 150 $^{\circ}$C for 10 minutes and immersed in 6M KOH aqueous electrolyte afterward the GO-CC composite was transformed to a graphene nanosheet on cotton cloth through annealing at 300 $^{\circ}$C for 2 hours in argon atmosphere (Figure 19). Table 3 Comparison of the specific capacitance between the GNSs-CC electrode and several GNSs-based electrodes [11].

Figure 18 Brush-coating of the graphene oxide ink on cotton cloth [11].
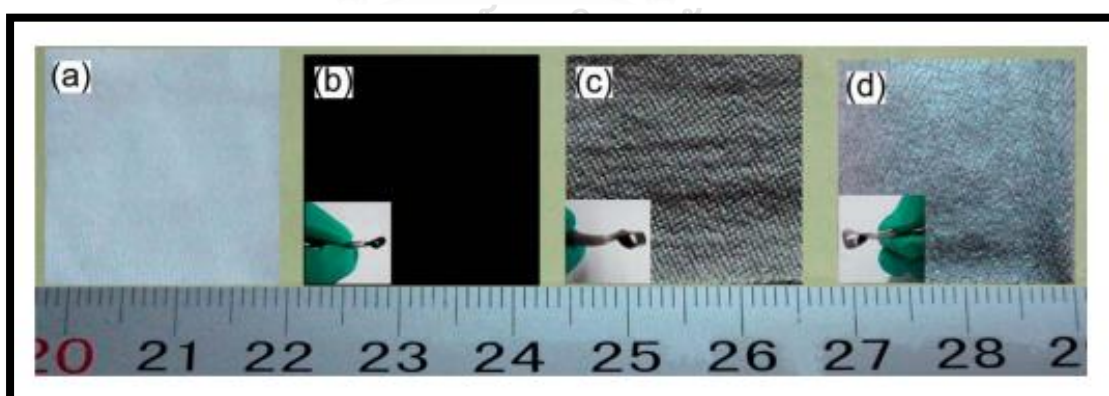
Figure 19 Photographs of pure cotton cloth (a) before and (b) after annealing at 300 $^{\circ}$C for 2 hour in an argon atmosphere, and the GO-coated cotton cloth (c) before and (d) after annealing [11]

Table 3 Comparison of the specific capacitance between the GNSs-CC electrode and several GNSs-based electrodes [11].

Type of material	Electrolye	Specific capacitance (F/g)
GNSs-CNT	1 M KCl	290.4
GNSs-MnO$_2$	0.1 M Na$_2$So$_4$	216
GNSs-MnO$_2$	1 M Na$_2$SO$_4$	210
GNSs-MnO$_2$	6M KOH	128
GNSs-CC	6 M KOH	326.8

GNSs-CC = graphene sheets (GNSs) – cotton cloth (CC)

2.5 Manganese oxide (MnO$_2$)

Pseudocapacitive (Faradic) reactions are charge storage mechanisms for manganese oxides that reactions occurring on the surface and in the bulk of the electrode. the surface adsorption of electrolyte cations (K+) involves the surface Faradaic reaction on the manganese oxide [27] according to equation 1.

$$(MnO_2)_{surface} + K^+ + e^- \rightarrow (MnOOC)_{surface} \qquad (1)$$

The bulk Faradaic reaction depends on the intercalation or deintercalation of electrolyte cations in the bulk of the manganese oxide to equation 2

$$MnO_2 + K^+ + e^- \rightarrow MnOOC \qquad (2)$$

The adjustment traced inactive materials mainly concerns high reversible capacitance, structural flexibility with stability, fast cation generating under high charge-discharge rates and natural amicability. As a progress metal component, manganese can exist as an assortment of stable oxides. [27].

Hu et al. [26] study of MnO$_2$ coated on SWCNTs cotton fiber the time required to charge the SCs for deposition is increased. (Figure 20left). The areal capacitance of the device reaches 0.41 F/cm^2. The specific capacitance of SWNT/cotton after MnO$_2$ are higher than SWNT/cotton without MnO$_2$ in Figure 20

middle. Such wearable SCs with salt electrolytes also show excellent cycling stability between the initial and the final specific capacitance over 35,000 cycles (Figure 20 right) [26].
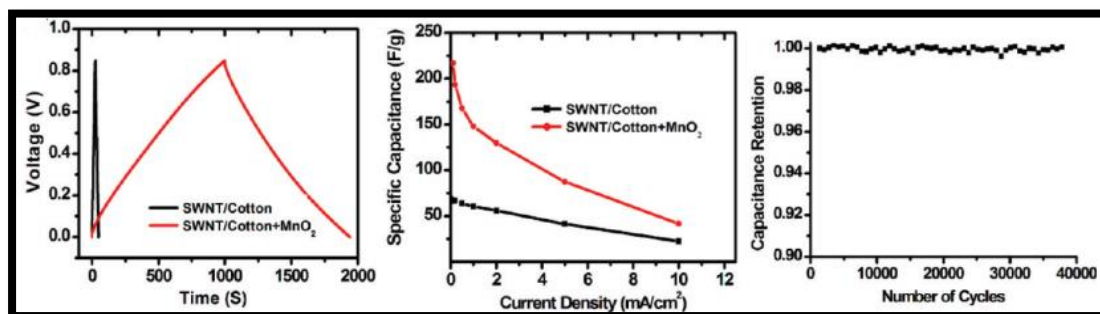
Figure 20 (Left) Charge-discharge of aqueous SC with SWNT/cotton electrodes and 2 M Li_2SO_4 as the electrolyte with the current of 20 µA/cm^2. The areal capacitance increases after MnO_2 deposition. (Middle) The specific capacitance of SWNT/cotton with and without MnO_2 for different discharge current densities. (Right) Cycling stability of an SC with SWNT-MnO_2 nanoparticles and porous textile conductor [26].

Nilesh R. Chodankar [28] used chemical bath deposition (CBD) to prepare porous nanostructured MnO_2 thin films by adding oxalic acid or critic acid in $KMnO_4$ and using Carboxymethyl cellulose-sodium sulfate (CMC-Na_2SO_4) gel electrolyte. Thin-film formation is based on the principle of controlled precipitation. The deposition of MnO_2 thin films involves several distinct steps such as nucleation, aggregation, coalescence and subsequently, the growth of particles leads to the film formation [28] and results of SEM in Figure 21.

B-MnO_2 film was prepared without a reducing agent but only dipped into the $KMnO_4$ solution. The chemical reaction for the growth of B-MnO_2 is as follows:

$$4MnO_4^- + 2H_2O \rightarrow 4MnO_2 + 4OH^- + 2O_2 \tag{3}$$

And O-MnO_2 (Oxalic) and C-MnO_2 (Citric) thin-film follow by equation 4 and 5 respectively
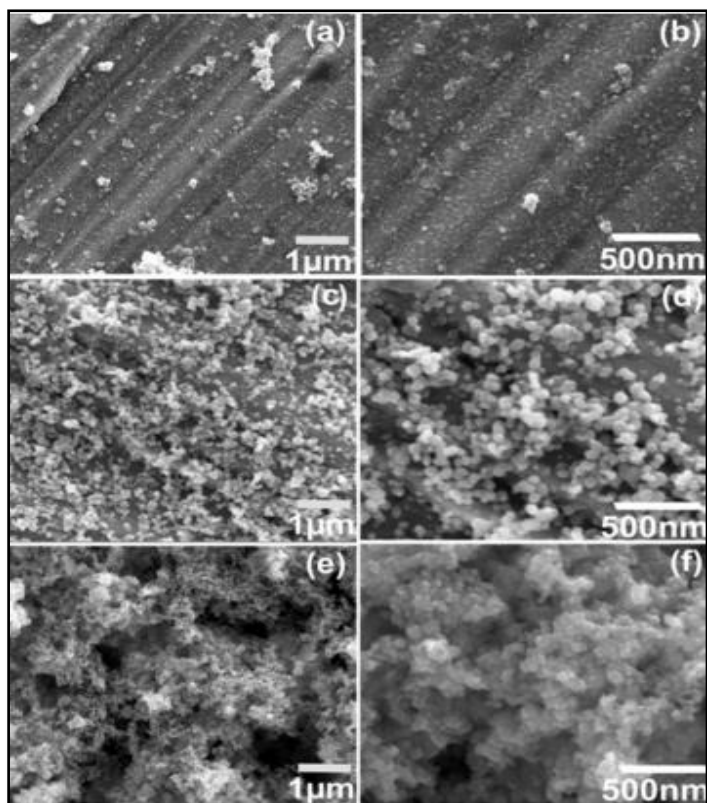
Figure 21 The SEM images of (a, b) B-MnO$_2$ (c, d) O-MnO$_2$ and (e, f) C-MnO$_2$ thin films at different magnifications [28]

$$10KMnO_4 + 3H_2C_2O_4 \rightarrow 3MnO_2 + 2KOH + 4H_2O + 6CO_2 \qquad (4)$$

$$10KMnO_4 + 3H_8C_6O_7 \rightarrow 6MnO_2 + 6KOH + 2H_2O + 6CO_2 \qquad (5)$$
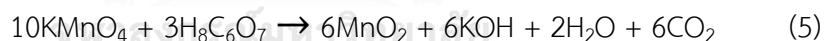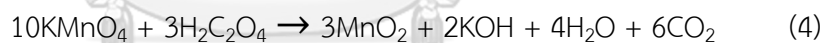
Table 4 The areal specific capacitance (mF/cm^2) and the specific capacitance(F/g) values of all samples at different scan rates [28].

B-MnO$_2$			O-MnO$_2$			C-MnO$_2$		
Scan rate (mV/s)	AC (mF/cm)	SC (F/g)	AC (mF/cm^2)	SC (F/g)	AC (mF/cm^2)	SC (F/g)
5	412	153	838	322	1609	643
10	394	146	757	291	1657	627
20	376	139	697	268	1525	610
50	330	122	638	245	1426	570

*AC = Areal capacitance, SC= Specific capacitance

The areal specific capacitance (mF/cm^2) and the specific capacitance(F/g) values of all samples at different scan rates are shown in table 4. Power density and energy density are shown in Figure 22-23. From Table 4 the areal capacitance and the specific capacitance increase when electrode uses KMnO$_4$ with citric solution.
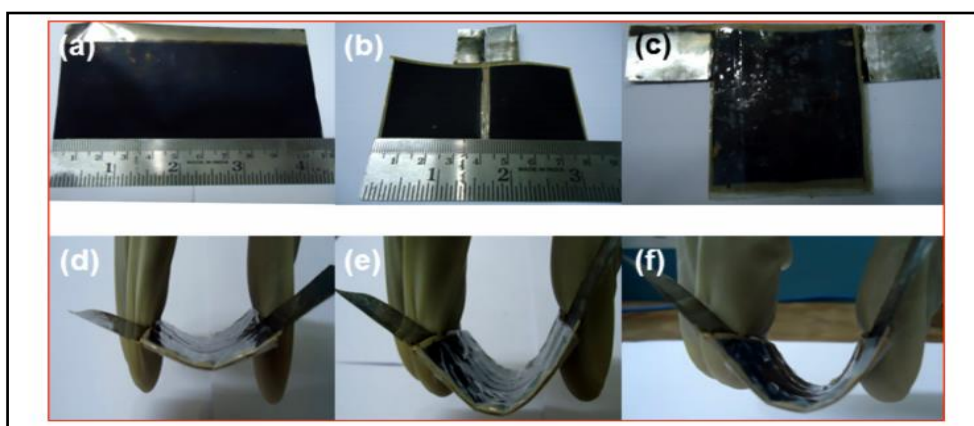
Figure 22 (a) The C-MnO$_2$ electrode (11.7 cm^2). (b) The two C-MnO$_2$ electrodes with a layer of CMC-NaSO$_4$ gel electrolyte. (c) Actual fabricated flexible-all-solid-state thin film symmetric supercapacitor. (d–f) The flexibility of the device at different bending angles [28].
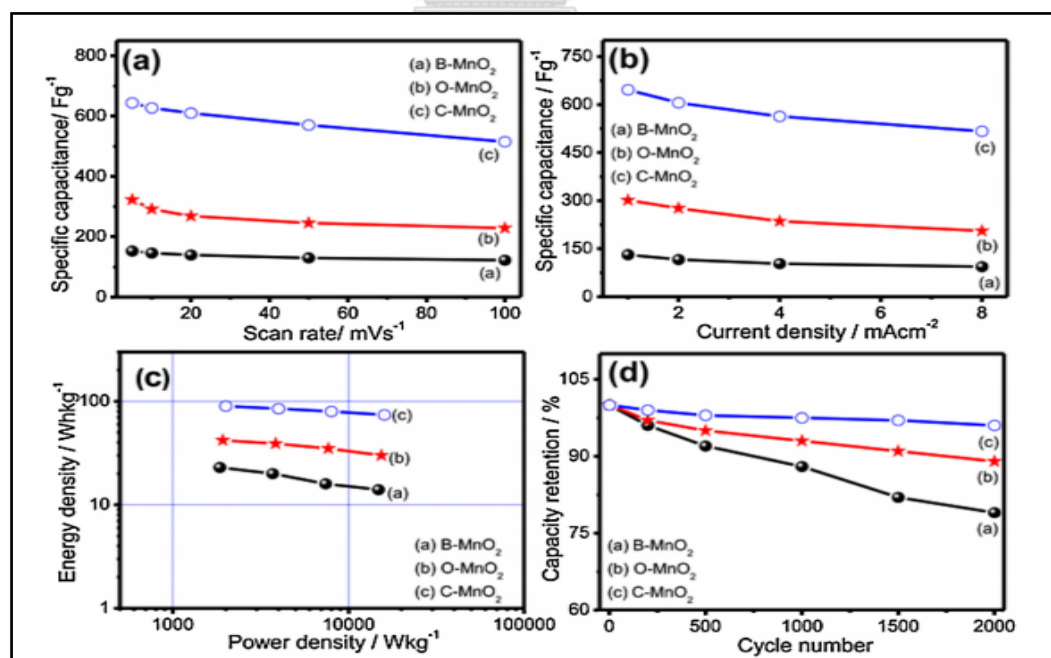
Figure 23 Specific capacitance of specimen with difference (a) scan rate and (b) current density. (c) Ragone plots and (d) capacity retention of B-MnO$_2$, O-MnO$_2$, and C-MnO$_2$ thin films [28].

Ying Chen et al. (Figure 24) synthesized the multi-wall carbon nanotube multi-wall (MWCNTs were synthesized by an aerosol-assisted chemical vapor deposition method and ground with $KMnO_4$ and add H_2SO_4 to synthesis of MnO_2/graphene/CNT hybrids by equation 6). [29]

$$4KMnO_4 + 3C + 2H_2SO_4 \rightarrow 4MnO_2 + 3CO_2 + 2K_2SO_4 + 2H_2O \qquad (6)$$
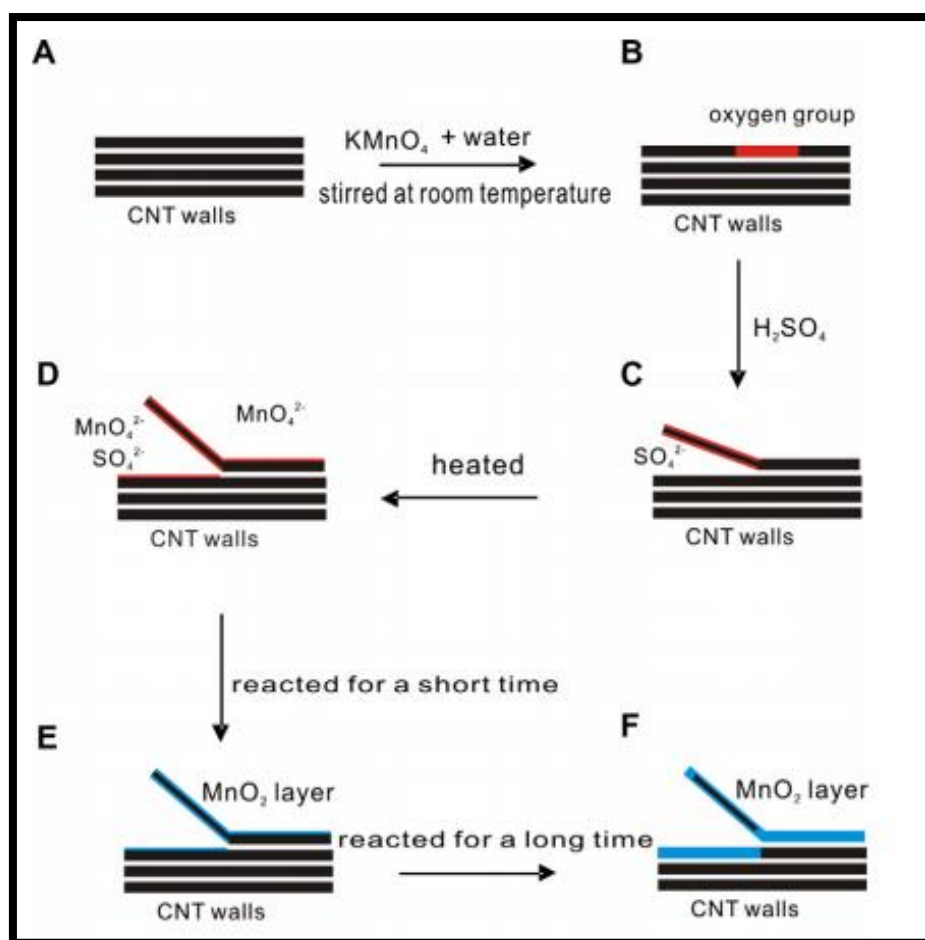
Figure 24 Schematic diagram of concept for the fabrication of the
MnO_2/graphene/CNT hybrid electrodes [29].

A sheet of cabon paper (CP) was coated with CNTs by dip-coating for 30 min. Afterward, the sample was denoted CP-CNT. Second, The solution for redox deposition is 0.25 M $KMnO_4$ with 0.5M H_2SO_4. The as-prepared CP-CNT and CP sheets

were immersed in $KMnO_4$ with H_2SO_4 solution for 30 minute. Thereafter, the samples were cleaned with distilled water. Finally two samples were prepared and denoted as CP–MnO_2 and CP–CNT–MnO_2. Figure 25 shows an image of the microfibrous CP with coated CNTs. CNTs are deposited on the microfibrous CP, either as networks, which form bridges between microfibers of CP Figure 26a and b or simply dispersed on the surface of the CP Figure 26a-b the thickness of MnO_2 deposited layer is 10 nm [30].
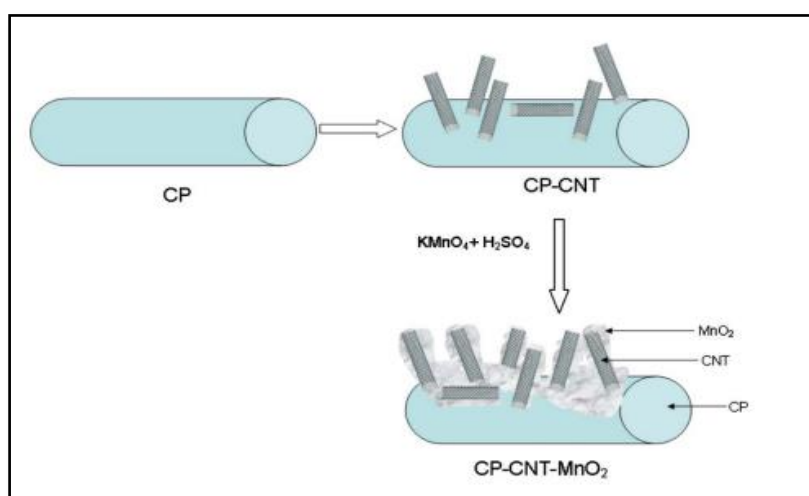
Figure 25 Concept for the fabrication of the CP, CP–CNT, and CP–CNT–MnO2 electrodes [30].
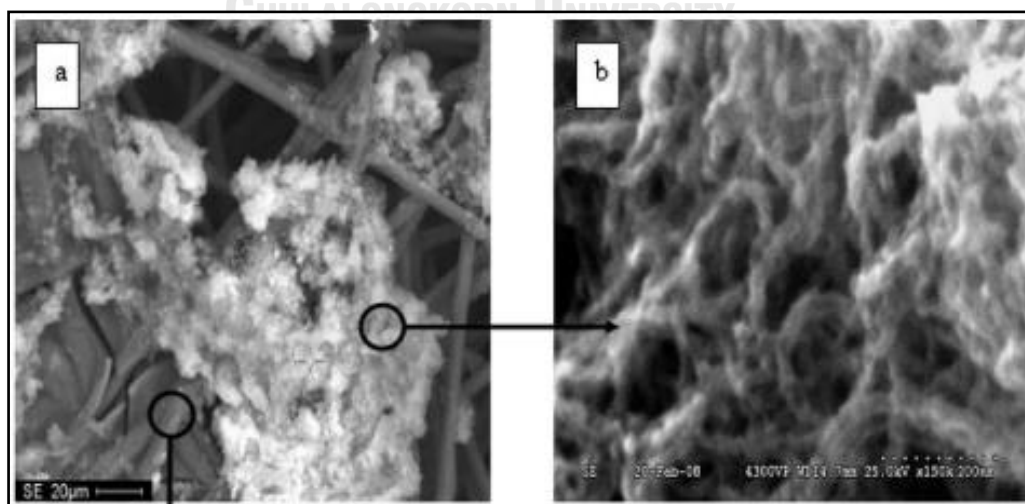
Figure 26 a–b SEM micrograph of the CP–CNT-MnO_2 nanocomposite [30].

In this thesis, there will be a preparation of Ag-CNTs, Ag-graphene, and Ag-CNT-graphene nanocomposites and their combination with MnO_2 bath deposition for flexible supercapacitor development. First, Ag-CNT, Ag-Graphene and Ag-CNT-Graphene will be prepared layered on the cotton cloth. Set 1) Supercapacitors are fabricated by 2 pieces of painted cotton. Set 2 Modified painted cotton cloth by MnO_2 bath deposition with 2 different solutions ($KMnO_4$ with citric acid and $KMnO_4$ with sulfuric acid) and at different times (15,30,45,60 min). The supercapacitor performance of Set 1 and Set 2 will be performed and evaluated.

Chapter 3

Experimental & Instrument

3.1 Materials

Textile ink (Normal Lemon Yellow 1006 – SCALA 99) was received from Scala Screen & Digital Co., Ltd., carbon nanotubes (CNTs) – MWNTs (purity 95 %, length 0.5-2 µm and diameter 30-50 nm) was purchased form XFNANO, Inc., China. Graphene nanosheet (purity 98 %, with thickness < 15 µm and film size 3-6 µm) was receive from Nanjing Nano Co. Ltd., China. Silver powder (5-10 µm) was bought from Wuxi Adams Technology Co., Ltd. (China). and cotton textiles were purchased from Wipaporn Fabric Ltd. (Thailand).

3.2 Surface treatment

The cotton fabrics were immersed in 1 M NaOH solution and boiled at 95 °C for 1 hour; washed with de-ionized water to remove any undesirable impurities such as oil and dust until getting neutral pH of the wet cotton and dried in a vacuum oven at 60 °C overnight. (Figure 27)
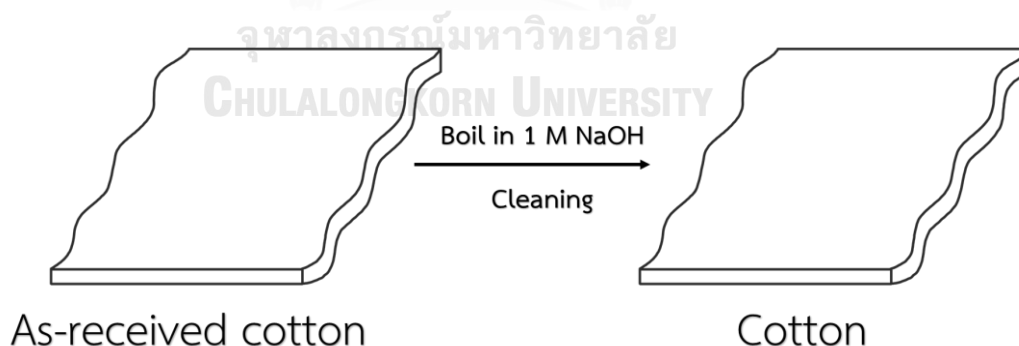
Figure 27 Pretreatment of cotton by 1 M NaOH.

3.3 Preparation of conductive cotton.

The cotton after cleaning with 1 M NaOH was used as a substrate for fabricated conductive cotton. After that, (I) The cotton was painted by the textile ink. and (II) The cotton was painted by the silver powder and the textile ink, which were mixed with ratio 1:1 %wt. as shown in Figure 28. The mass loading and resistance were measured.
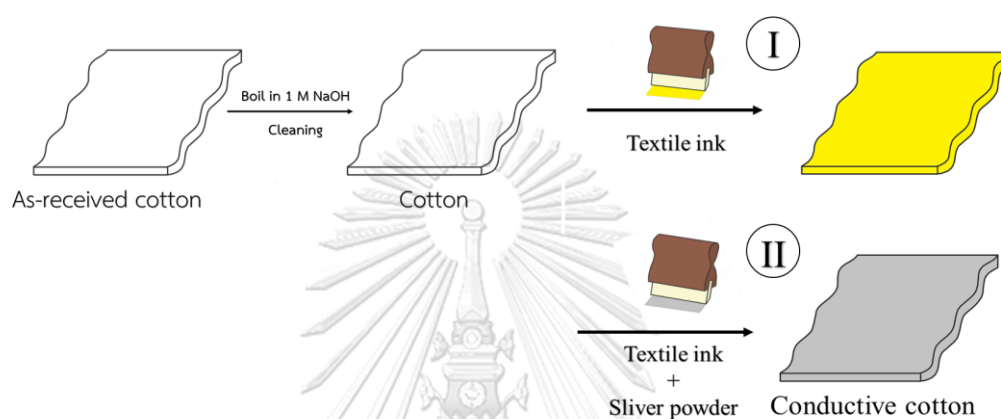
Figure 28 Schematic illustration for the fabrication of conductive cotton.

3.4 Preparation of conductive cotton electrode.

The conductive coating ink was prepared using silver powder (Ag) and textile ink with carbon nanotubes or graphene in different proportions and screen-printed on the cotton and dried under vacuum condition. The prepared conductive cotton electrode (CCE) specimens were denoted as 8AC, 6AC, 8AG, 6AG, 631AGC, 622 AGC and 613 AGC (where A stands for Ag; C for CNTs and G for graphene) according to the different volume ratios of the coating composition (Table 5).

Table 5 Compositions of the conductive coating ink prepared with different volume ratios using silver powder (Ag), carbon nanotubes (CNTs) and graphene.

Conditions	Sample Name	Ag (%V)	Graphene (%V)	CNTs (%V)
1	8AG	80	20	-
2	6AG*	60	40	-
3	8AC	80	-	20
4	6AC*	60	-	40
5	631AGC	60	30	10
6	622AGC	60	20	20
7	613AGC*	60	10	30

* MnO_2 was coated onto conductive cotton electrode

3.5 Preparation of conductive cotton electrode with MnO_2 coating

MnO_2 was coated onto conductive cotton electrode, CCE (6AG, 6AC and 613AGC) by bath deposition in area 1x4 cm^2 which consists of 2 groups of solution as follows (see also Figure 29).

1. Solution A: 0.03M $KMnO_4$ + 0.02 M Citric acid (Time 15, 30, 45 and 60 min)

2. Solution B: 0.03M $KMnO_4$ + 0.06 M Sulfuric acid (Time 15, 30, 45 and 60 min) After that, they were washed by DI water and dried in a vacuum oven at 60 °C overnight.

Chemical bath deposition
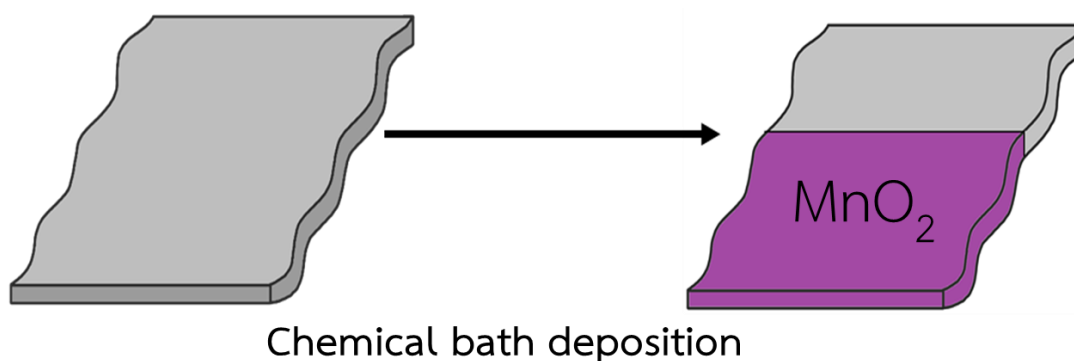
Figure 29 Chemical bath deposition of MnO_2.

3.6 Fabrication of flexible supercapacitors.
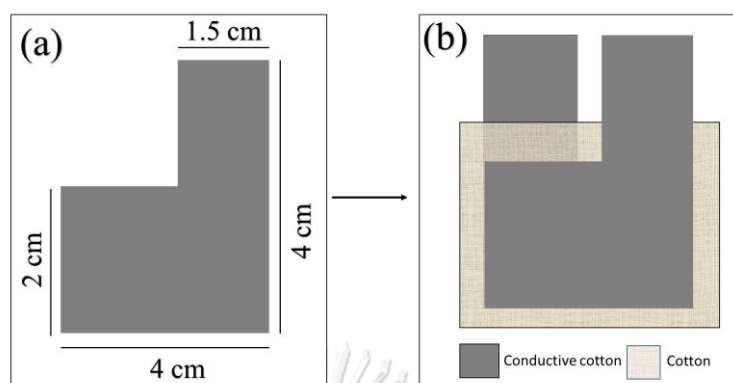
Figure 30 Schematic illustration for the fabrication of flexible supercapacitors, (a) electrode dimension, (b) device assembly

Furthermore, the prepared conductive cotton textile electrodes were fabricated as a flexible supercapacitor device, as illustrated in Figure 30. Figure 30 left depicts the design of the single piece of a flexible conductive cotton electrode and the cell assembly was executed using the two symmetric electrodes sandwiched together with the bare cotton fabric as the separator using the PVA-KOH gel electrolyte. Finally, the cell assembly was wrapped with an aluminum-based plastic foil through the heat sealer.

3.7 Characterization

The surface morphologies of the CCE specimens were observed by using a scanning electron microscope (SEM; Hitachi-S4800). The phase transformation of the CCE specimens was observed by using a X-Ray Diffractometer (XRD; burker D8 advance).

3.8 electrochemical performance

The symmetric two-electrode cell setup was employed for the galvanostatic charge-discharge (GCD) cycles using a Neware multi-channel battery system

(Shenzhen, China) at different current densities of 0.10 to 2.5 mA cm^{-2} in 6 M KOH electrolyte. The fabricated flexible supercapacitor device was characterized in a two-electrode system using cyclic voltammetry (CV) and GCD techniques using the Palmsens-4 instrument. The digital palm-size multi-meter (UNI-T; UT33C+) was used to measure the electrical resistance of the conductive cotton textiles.

Chapter 4

Results and discussion

4.1 Conductive cotton.
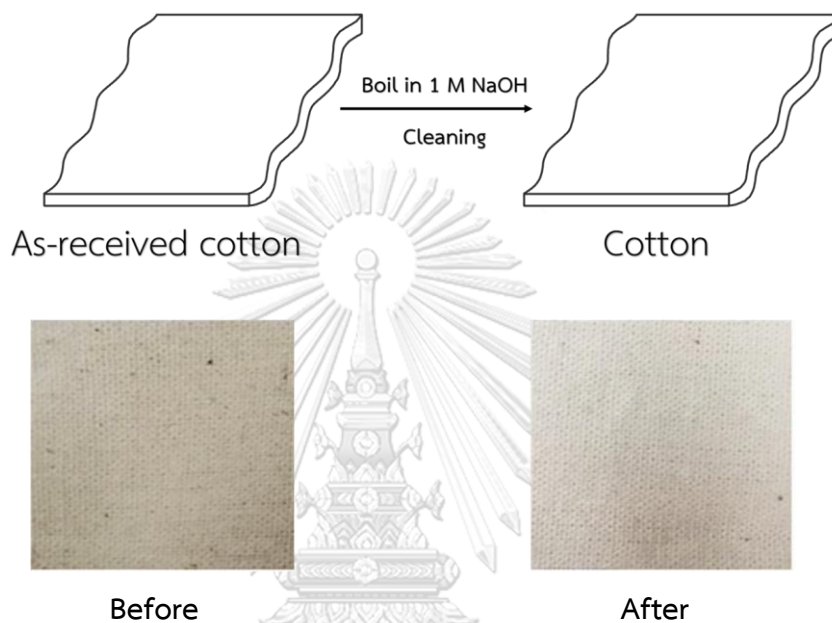
Figure 31 Before and after cleaning of cotton by boiling in 1 M NaOH.

The cotton fabric is pre-treated by immersing in 1 M sodium hydroxide (NaOH) at temperature of 95 °C for about an hour to remove impurities (oil and dust). Figure 31 shows as-received cotton before (left) and after cleaning (right). The treated cotton is brighter and cleaner. The thickness of cotton before and after cleaning is measured which their thickness are very similar (0.28 - 0.32 mm).
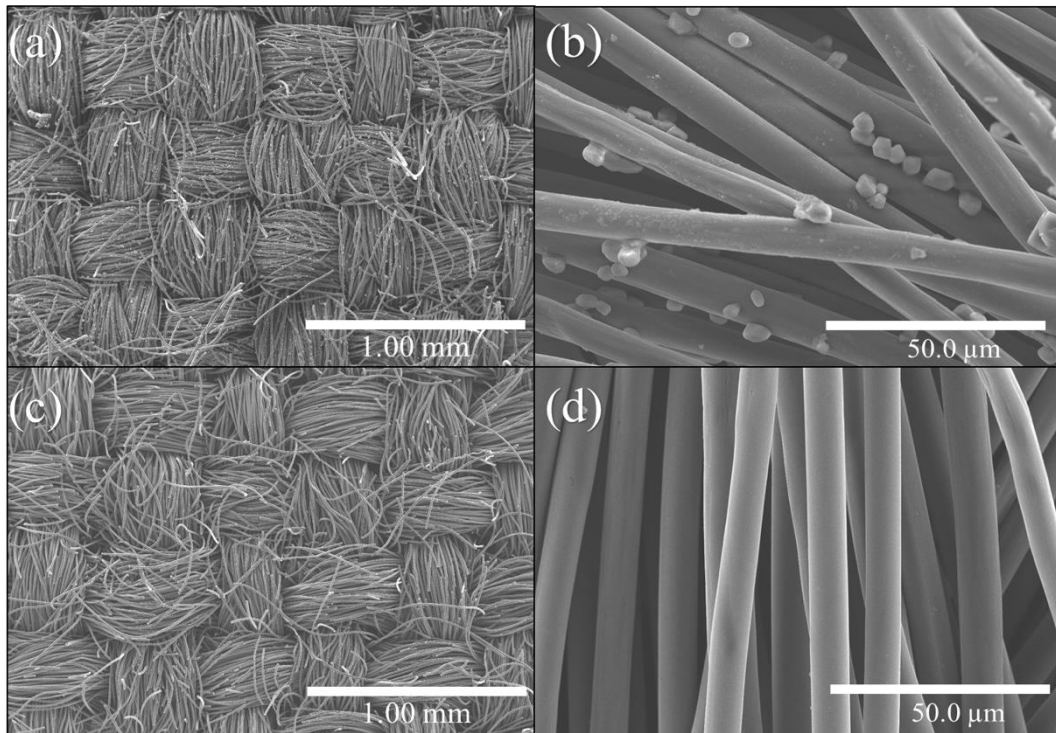
Figure 32 SEM images of cottons, (a) and (b) before washing, (c) and (d) after washing at different levels of magnification.

Before washing, it is found some dust on the as-received cotton surface (Figures 32 a) and 32b)). After washing, the cotton is brighter and cleaner than that of the as-received cotton because boiling with 1 M NaOH could remove oil and dust from the cotton surface (Figures 32 c) and 32 d)).

Then, textile ink and conductive ink, which consists of silver powder and textile ink (1:1 wt.% ratio), are screened onto the cotton. Figures 33 a) displays the SEM image of the pre-treated cotton clothes after washing and drying, which shows the fibrous woven cotton threads in the textile fabrics.

Figure 33 b) shows the SEM image of cotton clothes after coating by textile ink. This indicated the binder like clone to connect the cotton. Figures 33 c) and 33 d) shows the conductive cotton textile fabrication with a screen-printing method. The mixing between silver powder and textile ink which are the conductive coating layer. The layer is smooth and uniform coating with a little porous structure on the cotton fabric.
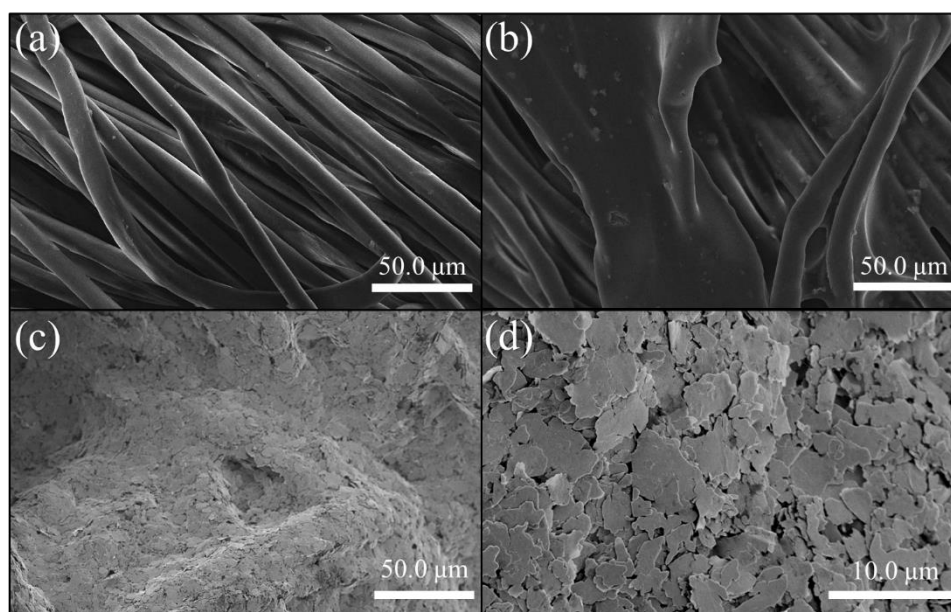
Figure 33 SEM images, a) cotton after washing by 1 M NaOH, b) textile ink coated on cotton, c and d) Ag and textile ink coated on cotton.

The measurement of the weight change (average mass loading) is shown in Table 6. The mass loading is 6.68 ± 4.23 and 21.52 ± 0.82 mg/cm^2 for the cotton after coated with textile ink and textile ink with silver powder, respectively. The mass loading of textile ink with silver powder is heavier since silver powder can deposit on the cotton surface. The electrical resistance of textile ink and conductive textile ink are also shown in Table 6. The fabricated cotton with conductive textile ink coating has low electrical resistance, which is only 13.636 ± 7.466 ohms/cm. However, it is not able to measure the resistance of the cotton with textile ink coating because of the excessive resistance.

Table 6 Mass loading and Resistance.

Sample name	Mass loading (mg/cm^2)	Resistance (Ω/cm)
Textile ink	6.68 ± 4.23	-
Textile ink + silver powder	21.52 ± 0.82	13.64 ± 7.466

Picture	Carbon	Oxygen	Silver
a) 50 μm	C Ka1_2	O Ka1	
b) 50 μm	C Ka1_2	O Ka1	
c) 50 μm	C Ka1_2	O Ka1	Ag La1
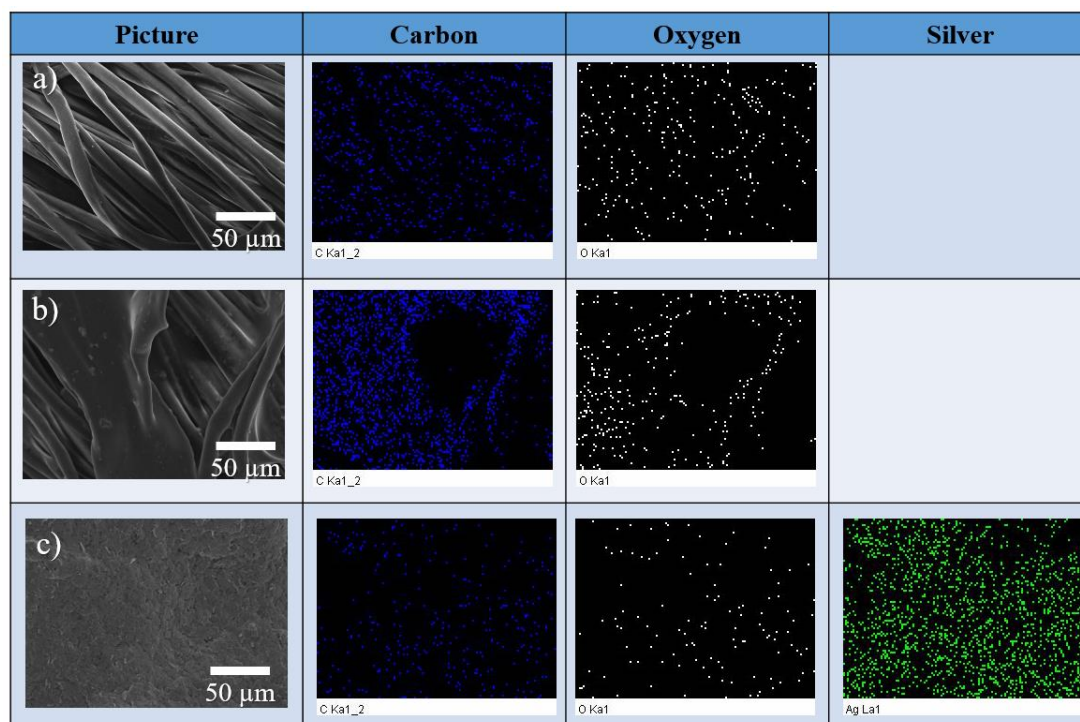
Figure 34 EDS images (a) cotton after washing by 1 M NaOH, (b) textile ink on cotton and (c) conductive cotton.

The energy-dispersive X-ray spectroscopy (EDS) mapping is utilized to inspect the elemental dispertion of cotton textile materials at different stages. Figures 34 a)-34 c) show the SEM images and the elemental distribution for the carbon (C), oxygen (O) and silver (Ag) sources appearing on the cotton, textile ink on cotton, and the silver powder applied to conductive cotton, respectively. It can be seen that the bare cotton and the textile ink cotton show uniform distribution of carbon and oxygen signals because of the alkaline treatment, as displayed in Figures 34 a) and 34 b), respectively. Figure 34 c) represents the uniform distribution of silver particles on the fabricated conductive cotton demonstrating that the silver particles are evenly distributed to the whole area of the coated cotton surface for better electrical conductivity.

4.2 Conductive cotton electrode (CCE)

4.2.1 Conductive cotton electrode: CNTs

The carbon nanotubes are used to modify conductive cotton and have a cylindrical nanostructure. Categories of the CNTs have two types, single-walled nanotubes (SWCNTs) and multi-walled nanotubes (MWCNTs). The MWCNTs have at least one external tubes progressively enveloping a SWCNT. The one-dimensional (1D) nanostructure invests individual CNTs with outstanding physical properties, such as a high thermal conductivity of 3500 W/m•K, charge mobility of 10,000 cm^2/V•s, Young's modulus of 1 TPa, and theoretical specific surface area of 1315 m^2/g [31].
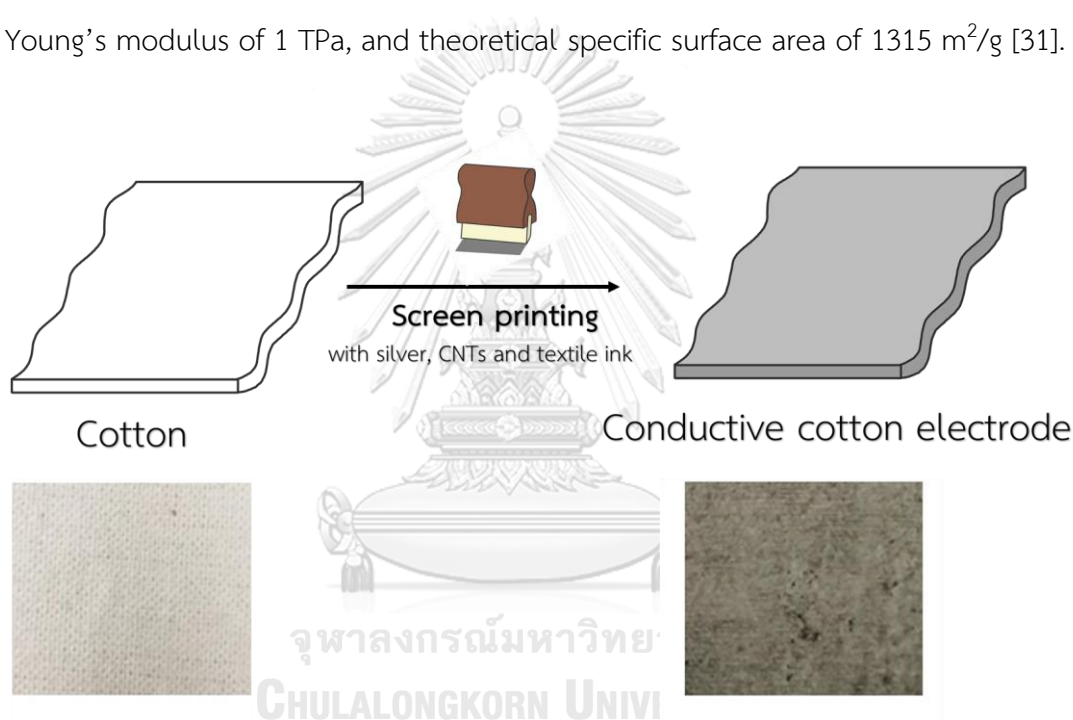
Figure 35 Schematic illustration for the fabrication process of conductive cotton electrode with textile ink, which consists of silver and carbon nanotubes.

Figure 35 depicts the fabrication procedure of the conductive cotton electrodes during various stages using the coating composition of silver and carbon nanotubes with textile ink as a binder. As it can be seen in Figure 36 a) 8AC, the surface of the cotton is covered by a layer of silver paricles and Figure 36 b) carbon nanotube (red arrow) can be successfully coated onto the cotton textile for the

flexible conductive sheet substrate. Similarly, the 6AC in Figure 36 c) and Figure 36 d) silver particles and carbon nanotubes can be deposited on the cotton.

The thickness of the 8AC and 6AC conductive layers do not vary significantly (0.092 ± 0.006 and 0.085 ± 0.007 mm for 8AC and 6AC, respectively). Comparing cotton with and without coating, these specimens have a similar thickness due to the uniform spreading of coating ink in the porous area of the cotton.

The mass loading of 8AC and 6AC are 26.56 ± 4.19 mg/cm^2 and 24.40 ± 4.59 mg/cm^2, respectively. Both thickness and mass loading have no significant difference with varying of coating compositions.
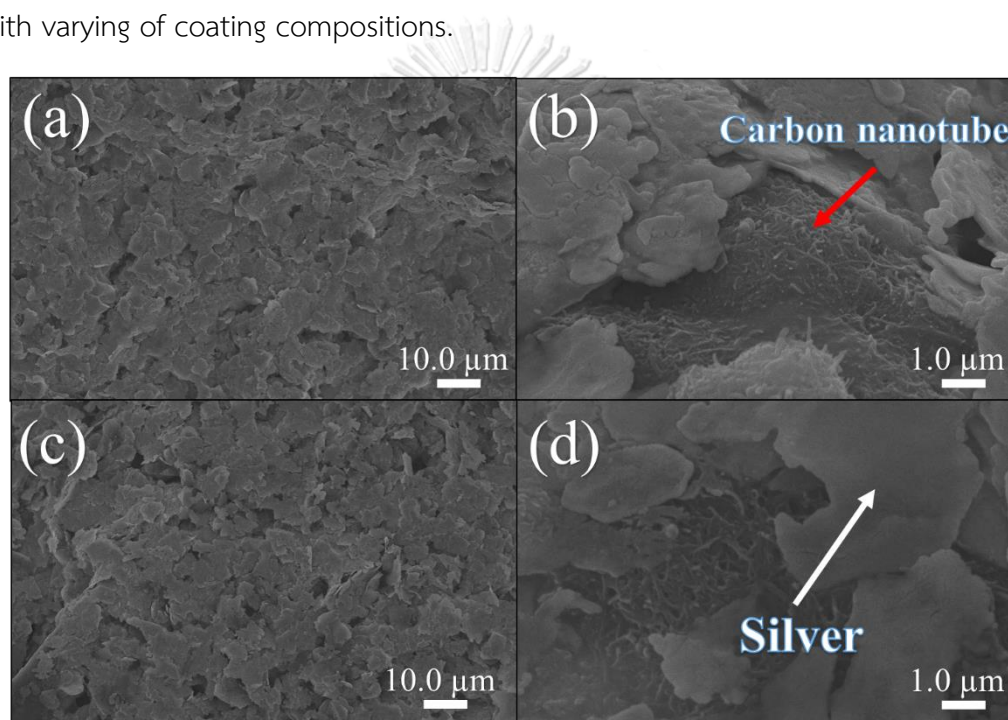
Figure 36 SEM images of conductive cotton electrode with different volume ratios of Ag and CNT (a) and (b) 80:20 (8AC); (c), and (d) 60:40 (6AC).

The resistance of CCE specimens with CNTs (8AC and 6AC) is 7.13 ± 2.61 and 6.82 ± 3.28 ohms/cm, respectively. The decreasing of silver particles does not affect resistance because the property (high electrical conductivity) of carbon nanotubes [31] affecting electrical resistance is not changed (comparing with conductive cotton only painting with Ag and textile ink (13.64 ± 7.47 ohms/cm).

Galvanostatic test (GCD) varying constant current density is used to investigate the value and behavior between voltage and time. An increase of voltage from 0 to

1 volt with increasing time demonstrates the electrical charging region. In contrast, a decrease of voltage from 1 to 0 volt with increasing time demonstrates the electrical discharging region. The GCD curves are measured at various current densities (0.1 to 2.5 mA/cm^2). In this work, they illustrate the triangle shape (see Figure 37). This indicates the electrical double layer charge storage behavior. The area of triangle shape would be decreased after adding more current density since electrons can be charged and discharged to the surface more rapidly. The GCD was calculated by equation (7) as follow:

$$C_s = \frac{It}{a\Delta V} \qquad\qquad (7)$$

Where C_s = specific capacitance (mF/cm^2), I = current (mA), a = area of conductive materials (in this work; 1 cm^2) and ΔV = voltage (V).

$$\text{Efficiency} = \text{discharge time/charge time} \qquad\qquad (8)$$

Figure 37 c) shows the GCD curve comparison of 8AC and 6AC conductive cottons. The curve of specimen 6AC is more nearly triangle than that of specimen 8AC. Moreover, with increasing current density from 0.1 to 2.5 mA/cm^2, the discharge time of 6AC is longer than that of 8AC. Therefore, specimen 6AC has better efficiency. To confirm this result, equation (8) is used to calculate efficiency. The increase concentration of carbon nanotubes enhances specific capacitance due to their theoretical specific surface area [31]. In addition, the ions in electrolyte can be increasingly diffused to area of electrode.

Table 7 Specific capacitance of specimens 8AC and 6AC.

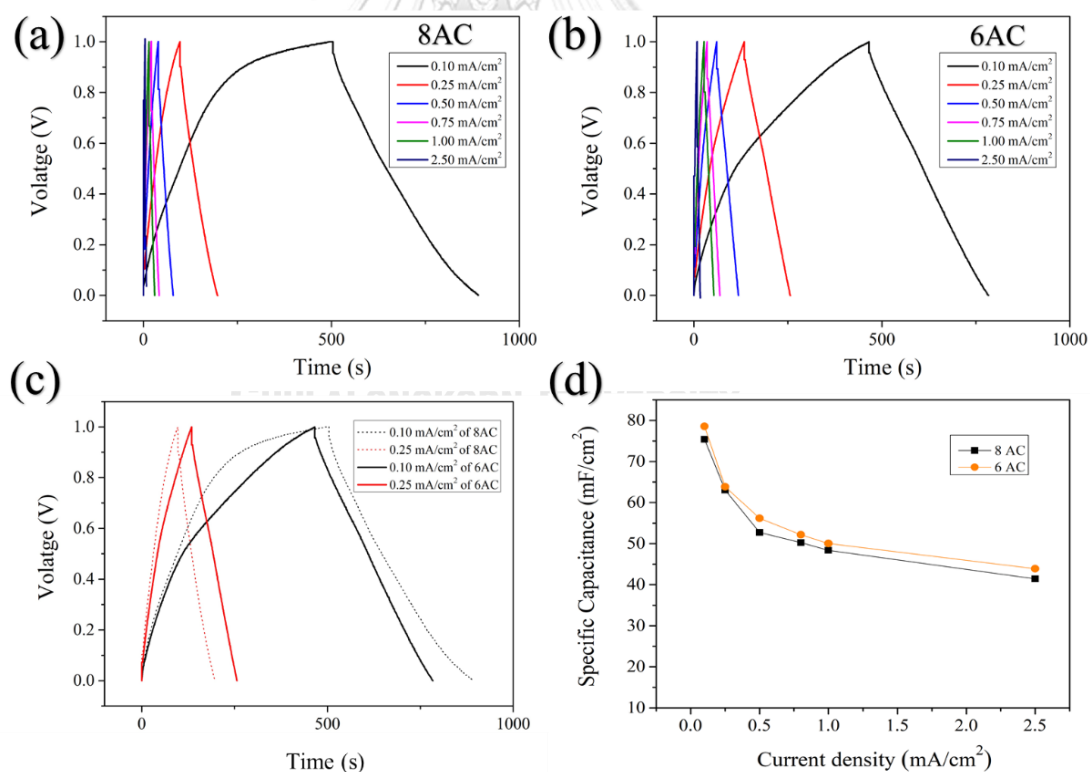| Current density	0.1 (mA/cm^2)	0.25 (mA/cm^2)	0.5 (mA/cm^2)	0.75 (mA/cm^2)	1 (mA/cm^2)	2.5 (mA/cm^2)
8AC (mF/cm^2)	75.42	63.05	52.73	50.25	48.35	41.43
6AC (mF/cm^2)	78.55	63.87	56.17	52.19	50.04	43.91

Figure 37 The GCD curves of (a) 8AC and (b) 6AC, (c) The GCD curve comparison of 8AC and 6AC at 0.10 and 0.25 mA/cm^2, (d) The specific capacitances of 8AC and 6AC.

4.2.2 Conductive cotton electrode: Graphene nanosheet

Graphene is a single layer of graphite, 2-D material. This structure can strongly influence on unique properties of graphene such as a high theoretical specific surface area (2630 m^2/g), outstanding conductivity, excellent chemical and thermal stability, large potential window and good mechanical flexibility. Graphene materials have been extensively explored as electrode materials for flexible supercapacitors [32-34].

Figure 38 depicts the fabrication procedure of the conductive cotton electrodes during various stages using the coating composition of silver and graphene nanosheet with textile ink as a binder. As it can be seen in Figure 38 a), 8 AG, the surface of the cotton is covered by a layer of silver. Figure 38 b) shows graphene nanosheet (red arrow) that can be successfully coated onto the cotton textile for the flexible conductive sheet substrate. Similarly, the 6AG in Figure 38 c) and Figure 38 d), silver powder and carbon nanotube can be deposited on the cotton. It is found that the thickness of the 8AG and 6AG conductive layer do not vary significantly (0.080 ±0.008 and 0.082 ± 0.015 mm for 8AG and 6AG, respectively) and the mass loading of 8AG and 6AG is 23.55 ± 4.61 mg/cm^2 and 25.71 ± 4.97 mg/cm^2, respectively. There is no significant difference in mass loading between specimens 8AG and 6AG.

The resistance of CCE specimens prepared with graphene nanosheets (8AG and 6AG) revealed the resistance of 68.19 ± 3.29 ohms/cm and 378.67 ± 70.44 ohms/cm, respectively. The resistance of CCE specimens (8AG and 6AG) can be enhanced due to the decreasing of silver particles. Moreover, the addition of graphene contents can extremely increase the resistance of CCE specimens (8AG and 6AG) due to the restacking phenomenon of graphene. During the manufacturing process, the aggregation and restacking of the graphene sheets are attributed to the interplanar π – π interactions and van der Waals forces between the graphene layers [33, 34].
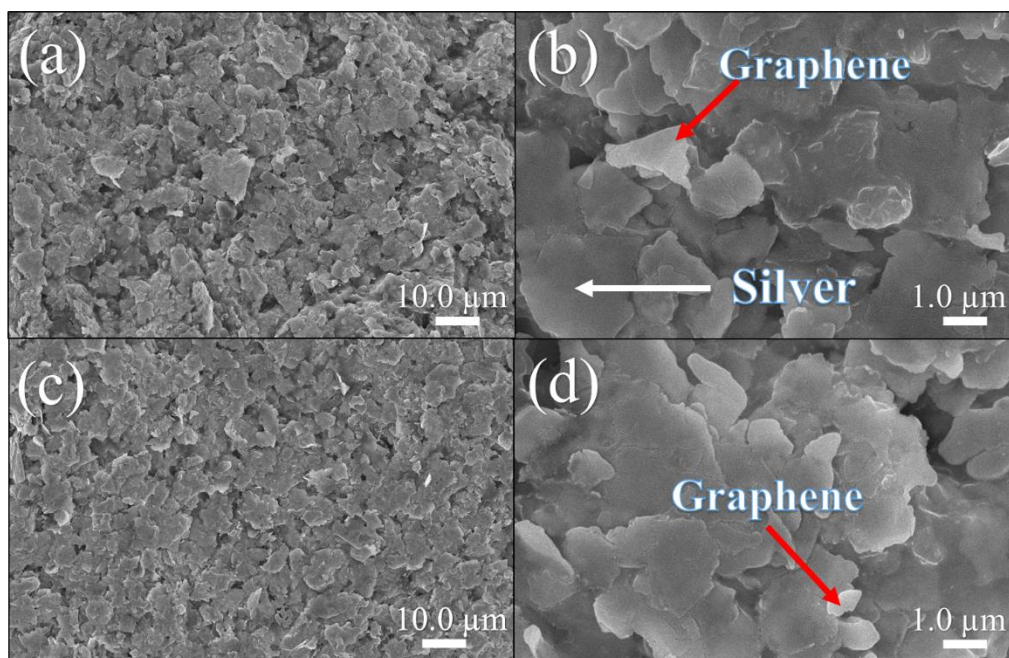
Figure 38 SEM images of the conductive cotton electrode with the different volume ratios of Ag and Graphene (a) and (b) 80:20 (8AG), (c), and (d) 60:40 (6AG).
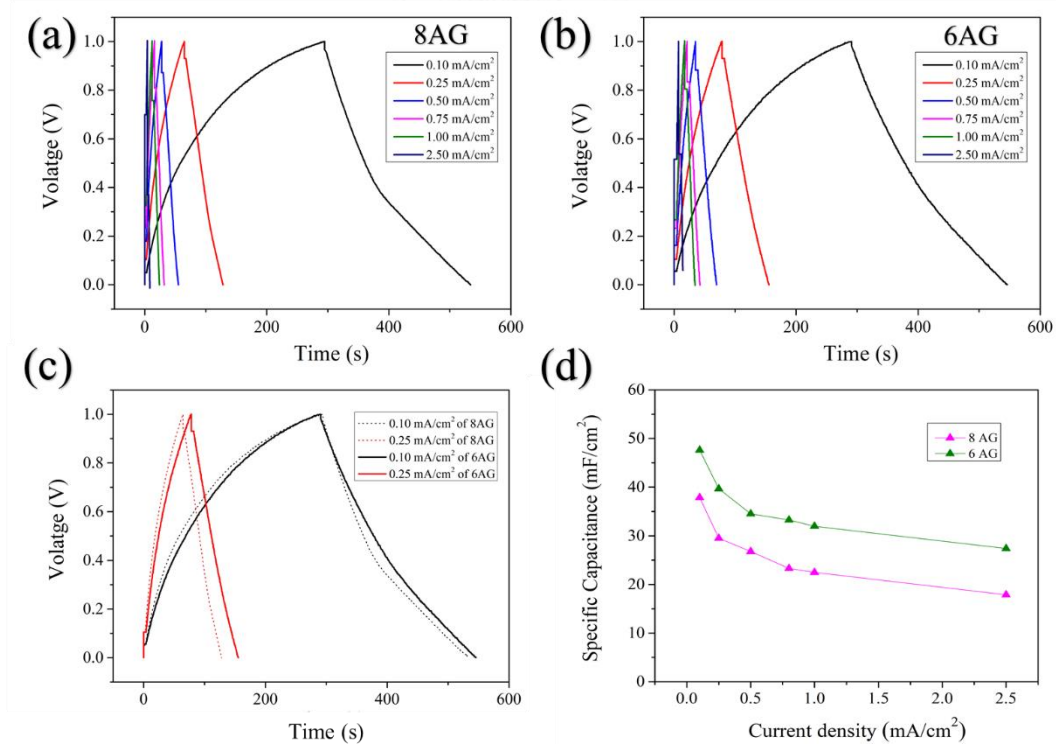
Figure 39 The GCD curve of (a) 8AG and (b) 6AG, (c) The GCD curve of 8AG and 6AG at 0.10 and 0.25 mA/cm^2, (d) The specific capacitances of 8AG and 6AG.

Figure 39 c) shows the GCD curves comparison of 8AG and 6AG conductive cottons. The curve of specimen 6AG is more nearly triangle than that of specimen 8AG. Moreover, with increasing current density from 0.1 to 2.5 mA/cm^2, the discharge time of 6AG is longer than the discharge time of 8AG. From equation 7 in the same current density, longer discharge time results in higher specific capacitance. Therefore, specimen 6AG has better efficiency since longer discharging time provides higher specific capacitance. To confirm this result, equation (8) is used to calculate efficiency.

Figure 39 d) and Table 8 display specific capacitances of specimens 6AG and 8AG. It is found that the specific capacitance of specimen 6AG is slightly more than 8AG (comparing with the same current density). The ions in electrolyte can be increasingly diffused to area affected by higher specific area. This results are shown when increasing graphene nanosheet. This would increase specific capacitance because graphene nanosheet can increase specific surface area. The specific capacitance, which consists of a higher concentration of graphene would provide higher specific capacitance.

Table 8 Specific capacitance of 8AG and 6AG.

Current density	0.1 (mA/cm^2)	0.25 (mA/cm^2)	0.5 (mA/cm^2)	0.75 (mA/cm^2)	1 (mA/cm^2)	2.5 (mA/cm^2)
8AG (mF/cm^2)	37.85	29.51	26.76	23.30	22.49	17.89
6AG (mF/cm^2)	47.63	39.68	34.52	33.26	31.95	27.40

4.2.3 Conductive cotton electrode: Mixture of CNTs and graphene nanosheet

From the previous section mentioned before, the specific surface area of graphene sheets are higher than CNTs. Therefore, the graphene/CNT composite electrodes are shown an advantage of large surface area of graphene sheets and excellent conductivity from CNTs [31].

The 631AGC cotton electrode is painted with 60% silver powder, 30% graphene and 10 % carbon nanotubes with textile ink. It is found that both graphene and carbon nanotubes are uniformly scattered on the cotton surface. Furthermore, higher carbon nanotubes in specimen 613AGC are found on the surface with applying with 60% silver powder, 10% graphene and 30 % carbon nanotubes (see Figure 40).
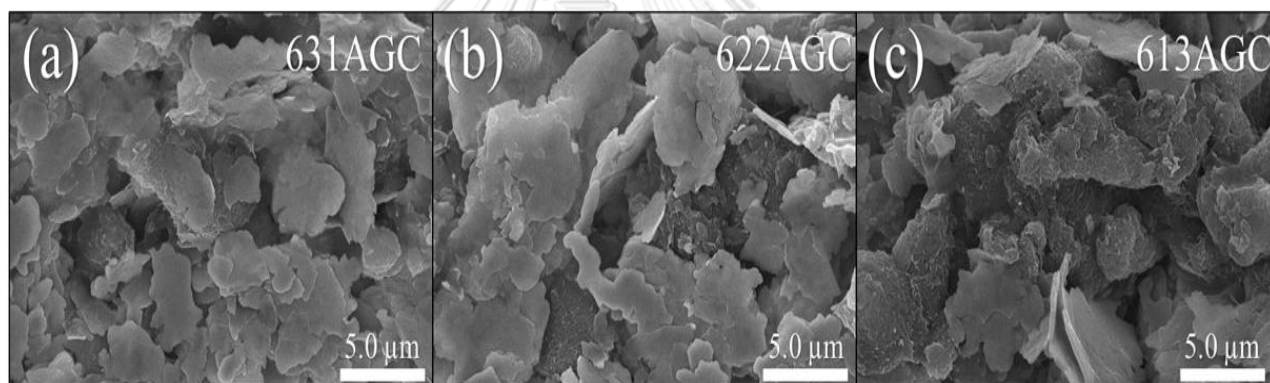
Figure 40 SEM images of conductive cotton electrode with different volume ratios of Ag with graphene and CNTs (a) 60:30:10 (631AGC), (b) 60:20:20 (622AGC), (c) 60:10:30 (613AGC)

The mass loading, thickness and resistance of the 631AGC, 622AGC and 613 AGC are shown in Table 9. The average mass loading is 28.11 ± 8.17, 24.69 ± 7.22 and 20.60 ± 3.75 mg/cm^2 for 631AGC, 622AGC and 613AGC, respectively. The thickness of the coating layer of 3 samples is not significantly different compared to as-received cotton (The thickness of the coating layer is about 0.01 mm (see Table 9)). The resistance of the CCE specimens (631AGC, 622AGC and 613AGC) fabricated

with graphene and carbon nanotubes are shown in table 9. Comparing the results of the three specimens, they are found that the specimens containing graphene provide more resistance than the specimen containing carbon nanotubes since carbon nanotubes have a good electrical conductivity [26]. Moreover, restacking of graphene nanosheets, leading to their agglomeration, can increase sheet resistance [33, 34].

Table 9 Mass loading, Thickness, Resistance of 631AGC, 622AGC and 613AGC

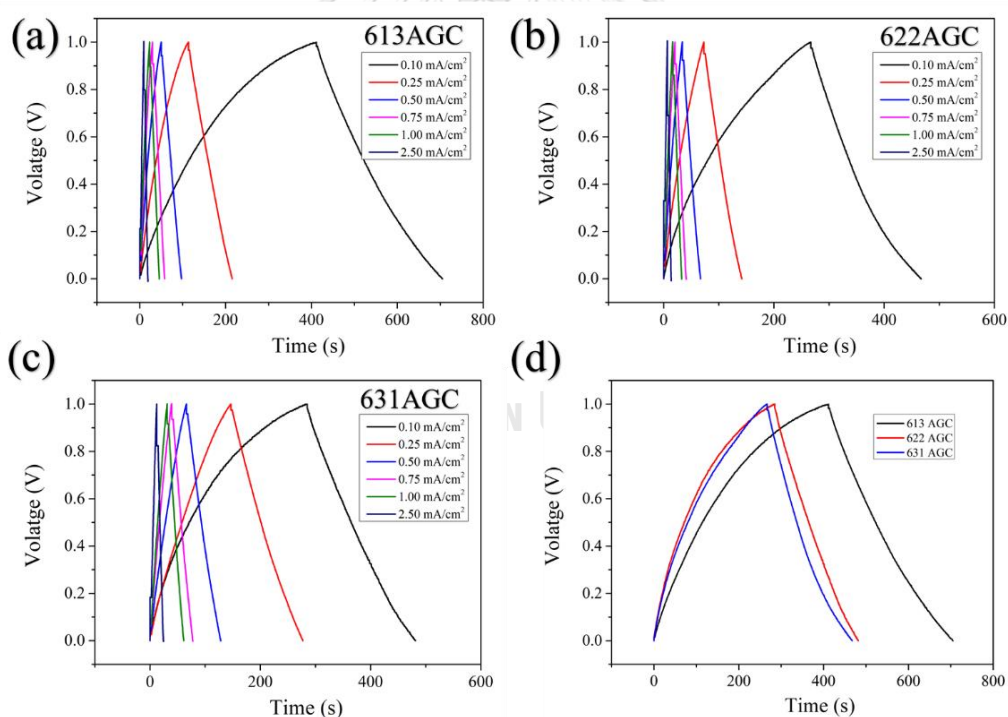| Sample Name	Mass loading (mg/cm^2)	Thickness (mm)	Resistance (Ω)
631AGC	28.11 ± 8.17	0.088 ± 0.008	40.893 ± 27.160
622AGC	24.58 ± 7.22	0.083 ± 0.009	11.760 ± 5.826
613AGC	20.60 ± 3.75	0.089 ± 0.011	4.656 ± 5.725

Figure 41 The galvanostatic charge-discharge (GCD) profiles at different current densities for (a) 613 AGC (60% silver + 10% graphene + 30% CNTs), (b) 622AGC (60% silver + 20% graphene + 20% CNTs), (c) 631AGC (60% silver + 30% graphene + 10% CNTs) and (d) The galvanostatic charge-discharge (GCD) profiles of 613 AGC, 622AGC and 631 AGC at 0.1 mA/cm^2

The galvanostatic charge-discharge (GCD) measurements are performed to investigate the electrochemical properties and specific capacitance values for the various types of conductive cotton electrodes fabricated with different concentrations of the mixture of CNTs and graphene. Figures 41 a) – 41 c) show the GCD results of 613AGC 622AGC and 631AGC with varying times. Figure 41 (d) shows the GCD results comparing among 613AGC, 622AGC and 631AGC data at low current density (0.10 mA/cm^2). It is found that specimen 613AGC spent longer time for the charge-discharge process, which influences on providing higher specific capacitance (see Figure 42). The specific capacitances are decreased by increasing of current density due to high current density does not give charges enough time to migrate through pores. That produces a lower specific capacitance compared to lower current density. For higher current density, the charge and discharge times are faster than lower current density which significantly decreases specific capacitance (equation 7, Figure 41 (GCD) and 42 (Specific capacitance)).
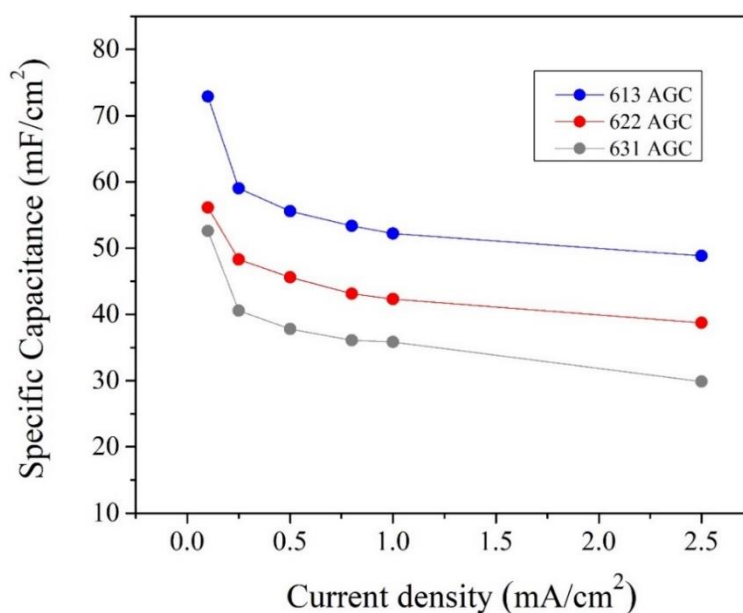

Figure 42 The specific capacitances of 613AGC, 622AGC and 631AGC specimens.

The specific capacitances of 613AGC, 622AGC and 631AGC at various current densities are shown in Table 10. The specific capacitance of 613AGC at various current densities are higher than those of 622AGC and 631AGC. The 613AGC specimen is the highest specific capacitance compared with others. The higher concentration of carbon nanotubes can provide higher specific capacitance because of the theoretical specific surface area of carbon nanotube [26, 31]. The higher specific surface area increases the diffusion rate of ions in electrolyte to the area. During the manufacturing process, the aggregation and restacking of the graphene sheets are attributed to the interplanar $\pi - \pi$ interactions and van der Waals forces between the graphene layers [33, 34]. The specific capacitance of 613AGC is higher specific than of 631AGC.

Table 10 Specific capacitances of 613AGC, 622AGC and 631AGC specimens

Current density (mA/cm^2)	Specific capacitance (mF/cm^2)		
	631 AGC	622 AGC	613 AGC
0.10	52.59	56.14	72.91
0.25	40.56	48.29	59.05
0.50	37.80	45.62	55.60
0.75	36.11	43.12	53.37
1.00	35.84	42.30	52.20
2.50	29.85	38.74	48.83

Figure 43 a) shows the specific capacitances of specimens contained a cotton with carbon nanotubes (CNTs) that are higher than those of specimens contained a cotton with graphene nanosheets because CNTs can disperse to a cotton and provide more conductivity than graphene nanosheets. A higher surface area of carbon nanotubes (CNTs) compared with graphene nanosheets results in specimens contained carbon nanotubes(CNTs) in electrolyte are more absorbent. As shown in figure 43 b), increasing of the amount of CNTs can increase the specific capacitance.
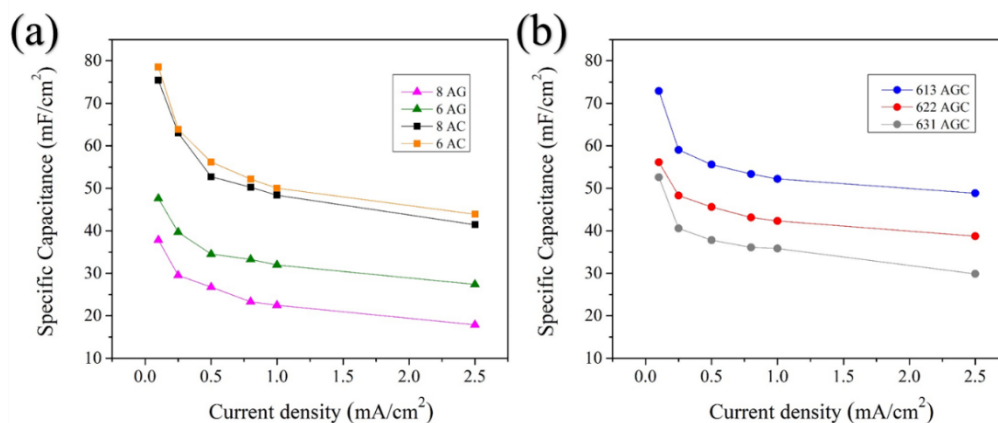
Figure 43 a) Specific capacitances of conductive cotton electrodes, which consist of silver and carbon nanotube (8AC and 6AC) and silver with graphene (8AG and 6AG) b) Specific capacitances of conductive cotton electrodes, which consist of silver with graphene and carbon nanotube.

The cotton with carbon nanotubes provides higher specific capacitance than that of graphene nanosheet since the carbon nanotubes are much smaller size than graphene nanosheet. It is very effective way by adding CNTs in conductive cotton and providing higher specific capacitance.

4.3 Conductive cotton electrodes with MnO_2 coating: $KMnO_4$ with citric acid

4.3.1 Conductive cotton electrodes with MnO_2 coating: $KMnO_4$ with citric acid.

Chemical bath deposition (CBD) is a easy method and low-cost for prepare electrode of MnO_2 materials. CBD is simple to prepare large scale of materials with divers surface morphologies. [28].

After the method mentioned above (section 4.2), the CCE can be also improved to increase the specific capacitance by adding MnO_2 in the electrode by chemical bath deposition. $KMnO_4$ with citric acid ($H_8C_6O_7$) solution is used for immersing the conductive cotton. The conductive cotton after immersing in $KMnO_4$ with citric acid solution at various times is shown in Figure 44.
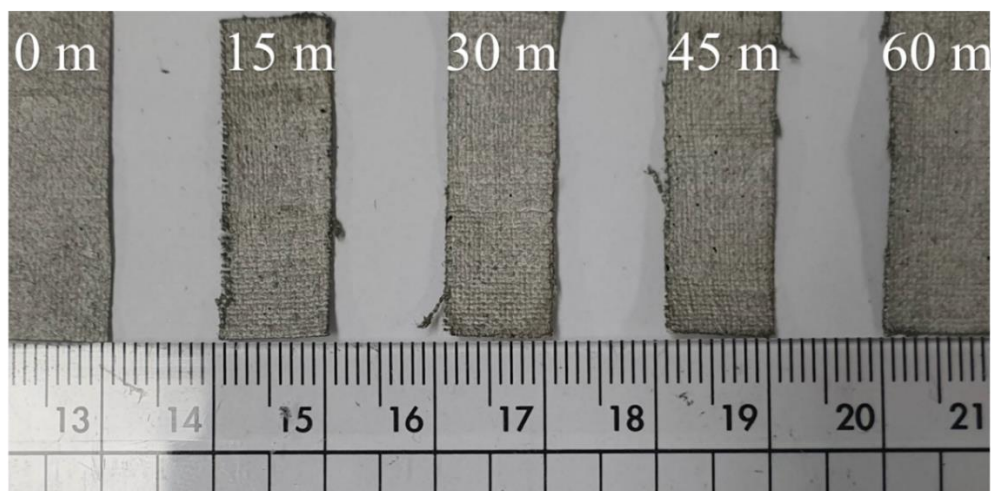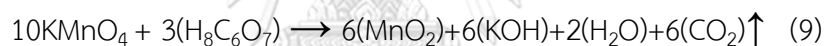
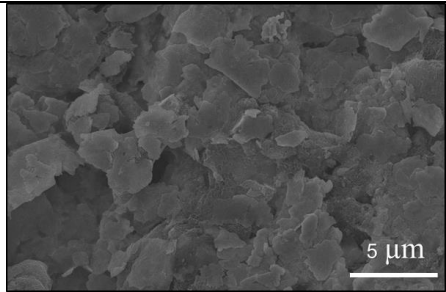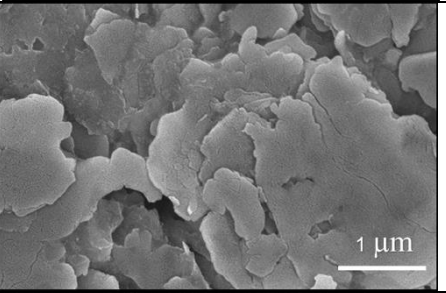**Figure 44** Conductive cotton (6AC), immersing in $KMnO_4$ with citric acid with various times (15-60 minutes)
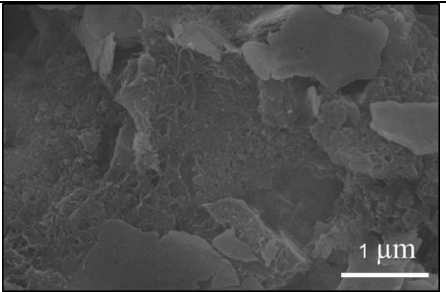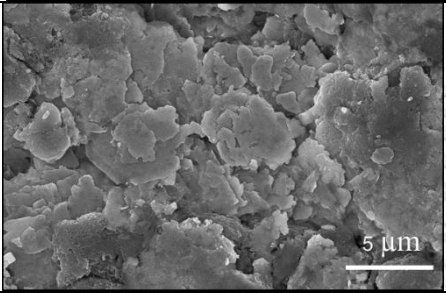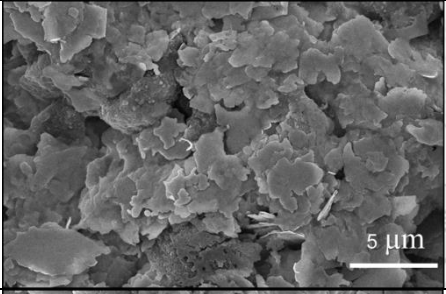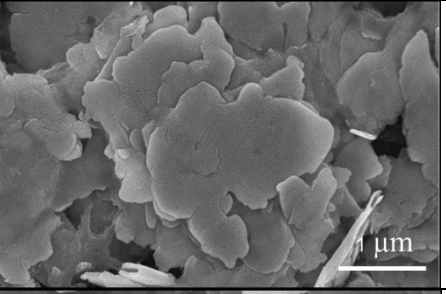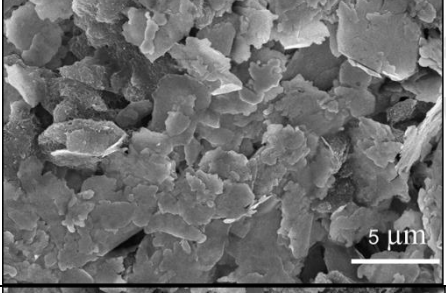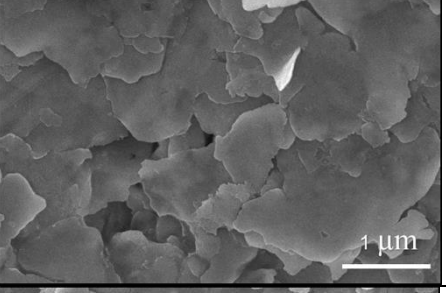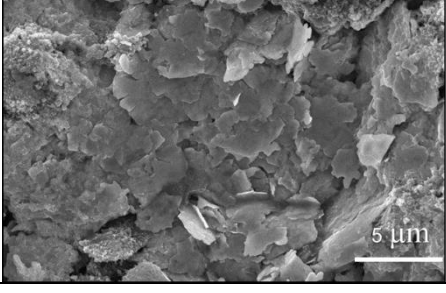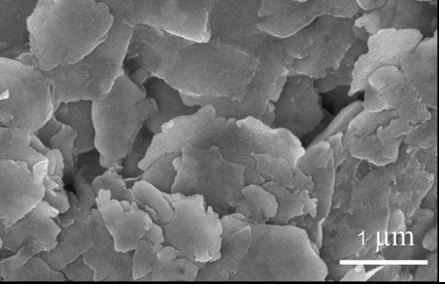
When citric acid ($H_8C_6O_7$) is added to $KMnO_4$, MnO_2 powder would be produced as the chemical reaction, which is shown in equation 9.

$$10KMnO_4 + 3(H_8C_6O_7) \longrightarrow 6(MnO_2)+6(KOH)+2(H_2O)+6(CO_2)\uparrow \quad (9)$$

Conductive cotton is improved by $KMnO_4$ with Citric acid. Figure 44 shows conductive cotton (6AC) immersed in $KMnO_4$ with Citric acid solution. This picture indicates that 6AC-C15 to 6AC-C60 specimens do not significantly change both the color and thickness before and after immersing in $KMnO_4$ + citric acid solution. Moreover, the obtained results indicate a slight decrease in mass loading of the conductive cotton mass loading.

Table 11 shows SEM images of the conductive cottons of 6AC-C15 to 6AC-C60. The microstructure of 6AC (carbon nanotube with silver powder and textile ink), before immersing in $KMnO_4$ with the citric acid solution, consists of plane-stacked morphology covering the cotton. However, after immersing 6AC in $KMnO_4$ with a citric acid solution, the morphology on the conductive layer of the cotton surface did not change because the conductive layer, which consists of silver particles, is stable and did not interact with MnO_2 powder. Thus, MnO_2 powders, synthesized using equation 9, could not be deposited on the surface.

Table 11 SEM images of conductive cotton after immersing in KMnO$_4$+Citric acid solution

	X 500	X 10,000
6AC		
6AC-C15		
6AC-C30		
6AC-C45		
6AC-C60		

The mass loading of 6AC conductive cotton (silver powder, carbon nanotube and textile ink) decreased to 1.83 ± 2.41, 2.05 ± 0.47, 1.34 ± 0.72 and 1.72 ± 0.81 after immersing in $KMnO_4$ with Citric acid at 15, 30, 45 and 60 min, respectively due to the erosion of solution on the conductive layer. Table 12 shows similar results of the mass loading of all specimens (6AC, 6AG, and 613AGC). The thickness of conductive cotton before and after immersing in $KMnO_4$ with a citric solution is very similar (no significant change).

Table 12 Mass loading of conductive cotton after immersing in $KMnO_4$ with citric solution

Sample	Mass loading mg/cm^2	Sample	Mass loading mg/cm^2	Sample	Mass loading mg/cm^2
6AC-C15	-1.83 ± 1.41	6AG-C15	-1.79 ± 1.72	613AGC-C15	-1.93 ± 0.28
6AC-C30	-2.05 ± 0.47	6AG-C30	-2.48 ±0.55	613AGC-C30	-2.93 ± 0.24
6AC-C45	-1.34 ± 0.72	6AG-C45	-1.98 ± 1.91	613AGC-C45	-2.35 ± 0.48
6AC-C60	-1.72 ± 0.81	6AG-C60	-1.67 ± 0.94	613AGC-C60	-2.46 ± 0.37
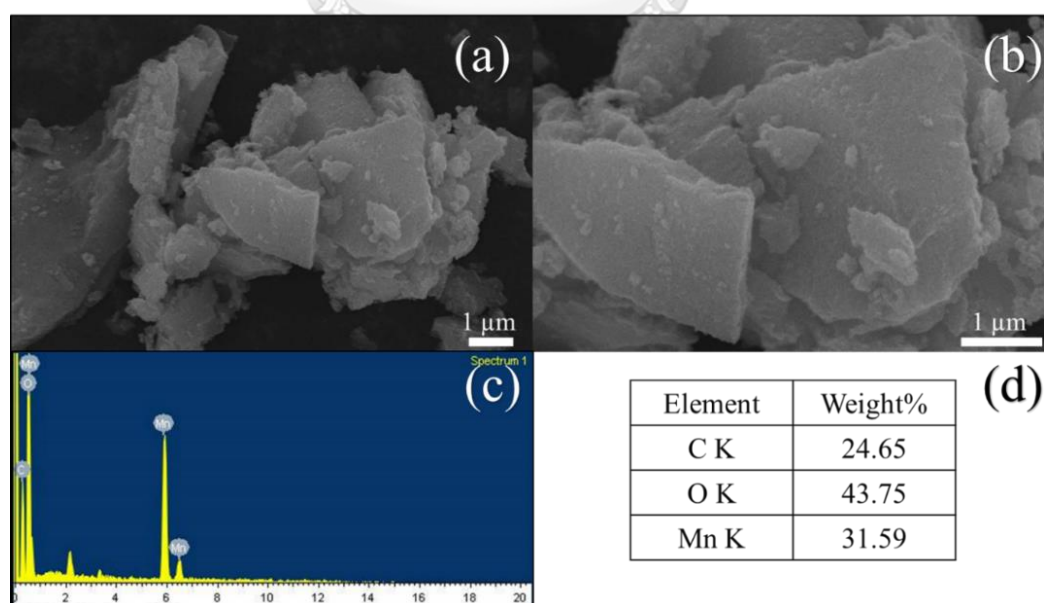
Figure 45 a) and b) The MnO_2 powder synthesized using equation 9, c) and d) chemical composition of MnO_2 powder.

The MnO_2 powders (from equation 9) are seen in Figures 45 a) and 45 b). Figure 45 c) shows the EDS measurement of Manganese (Mn) and Oxygen (O). Carbon is also detected and found because of using carbon tape to increase the electrical conductivity of specimens for investigation by SEM.

The energy-dispersive X-ray spectroscopy (EDS) is used to examine the element distribution of the conductive cotton at various stages. Figure 46 and Table 13 display the SEM images and the corresponding elements for the only carbon (C) oxygen (O) and silver (Ag) sources appearing on the 6AC-15 and 6AC-60. The chemical composition of 6AC-15 is 14.60 wt.%C, 2.81 wt.%O, 82.60 wt.%Ag while 6AC-60 is 16.42 wt.%C, 5.98 wt.%O and 77.60 wt.%Ag. As it can be seen in Figure 46 (bottom), Manganese (Mn) cannot be detected since MnO_2 powders could not be to deposited onto the cotton.
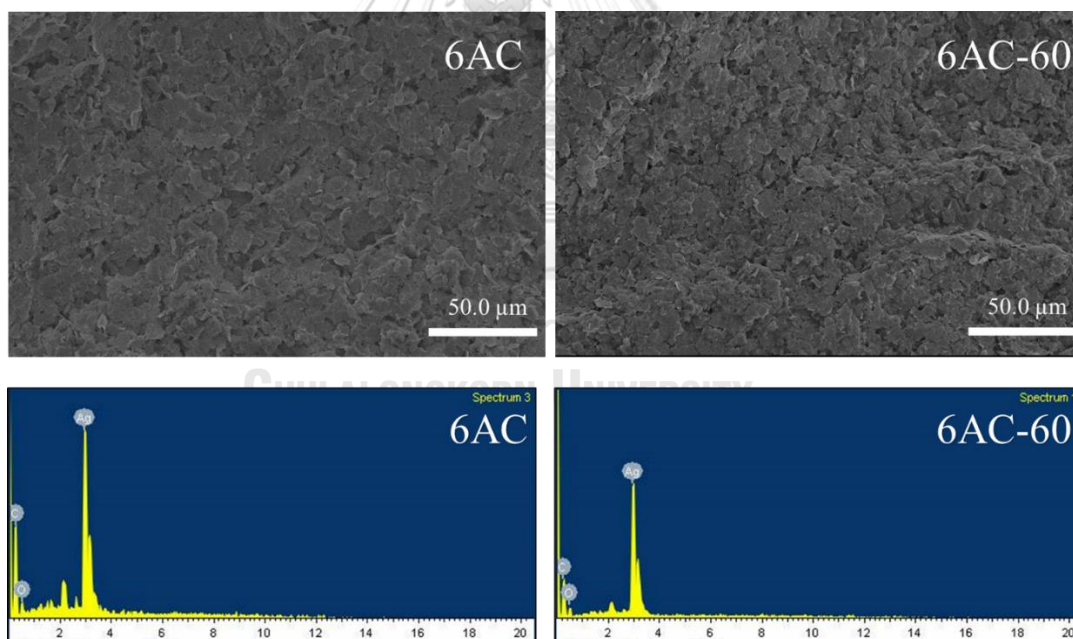
Figure 46 (Top) SEM images of 6AC and 6AC-C60 and (Bottom) EDS elements of 6AC and 6AC-C60 specimens.

Table 13 EDS measurement of conductive cotton before and after immersing in $KMnO_4$ with citric acid solution for 60 minutes.

	Weight%	
Element	6AC-15	6AC-C60
C K	14.60	16.42
O K	2.81	5.98
Ag L	82.60	77.60

The X-ray diffraction (XRD) analysis is performed to confirm the crystal structure of 6AC-15 to 6AC-60 final products as presented in Figure 47.

The XRD peak at the 2θ values of 38.166^o, 44.277^o, 64.426^o and 77.472^o corresponding to the (1 1 1), (2 0 0), (2 2 0) and (3 1 1) crystal planes of silver are matched with the reported values from the Joint committee on Powder Diffraction Standards card (JCPDS card no.44-0141). The XRD peak at the 2θ values of 28.851^o, 56.629^o, 57.361^o and 59.767^o of Manganese dioxide (JCPDS card no.50-0866) is not found on the 6AC-C15 to 6AC-C60.
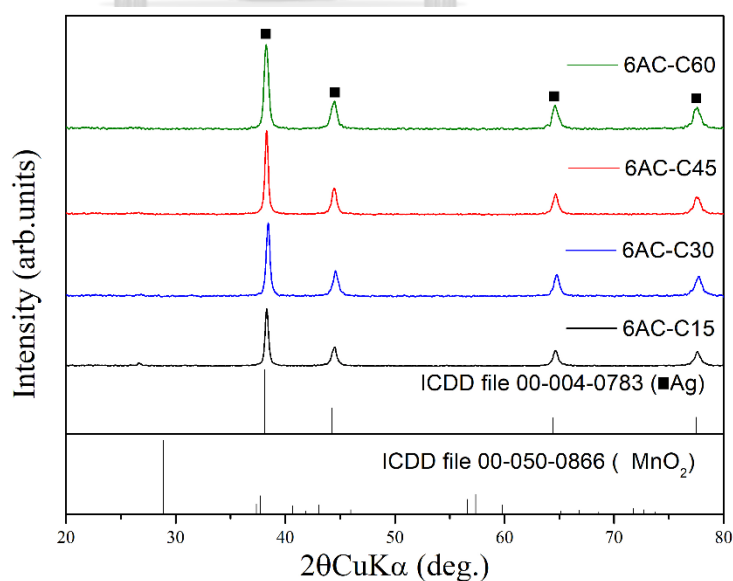
Figure 47 XRD patterns of 6AC-C15 to 6AC-C60 specimens.

The specific capacitances of 6AC-C15 to 6AC-C60 are shown in figure 48 and Table 14. At current density of 0.1 mA/cm^2, the specific capacitances of 6AC-C60 and 6AC-C45 are 323.17 and 312.83 mF/cm^2, respectively. The specific capacitances of 6AC-30 and 6AC-15 are 164.05 and 144.19 mF/cm^2, respectively. As shown in figure 48, they can be found that the highest specific capacitance for any current densitiy can be achieved in the conductive cotton immersed in KMnO$_4$ with citric acid at 60 minutes (6AC-C60). Therefore, the longer time of immersing in KMnO$_4$ with citric acid provides higher capacitance. This is due to that KOH can be chemical activation of carbon, which creates mesopore and micropore as well as make high specific surface area.

Figure 48 The specific capacitances of 6AC-C0 to 6AC-C60 specimens.

Table 14 The specific capacitances of 6AC-C0 to 6AC-C60 specimens.

Current density (mA/cm^2)	Specific capacitance (mF/cm^2)				
	6AC	6AC-15	6AC-30	6AC-45	6AC-60
0.1	78.55	144.19	164.05	312.83	323.17
0.25	63.87	94.37	156.95	277.9	271.20
0.5	56.17	81.04	137	192.3	238.47
0.75	52.19	77.66	133.05	166.6	206.05
1	50.04	76.77	130.05	156.47	190.30
2.5	46.91	77.02	114.05	155.05	189.75

The specific capacitances of 6AG-C15 to 6AG-C60 are shown in figure 49 and Table 15. At current density of 0.1 mA/cm^2 the specific capacitances of 6AG-C60 and 6AG-C45 and 112.20 and 87.42 mF/cm^2, respectively. The specific capacitances of 6AG-30 and 6AG-15 is 92.13 and 90.00 mF/cm^2, respectively. As shown in figure 49 they can be found that the highest specific capacitance for any current density can be also achieved in the conductive cotton immersed in KMnO$_4$ with citric acid at 60 minutes (6AG-C60). Therefore, the longer time of immersing in KMnO$_4$ with citric acid provides higher capacitance. This is due to that KOH can be chemical activation of carbon, which creates mesopore and micropore as well as make high specific surface area.

Figure 49 The specific capacitances of 6AG-C0 to 6AG-C60 specimens.

Table 15 The specific capacitance of 6AG-C0 to 6AG-C60 specimens.

Current density (mA/cm^2)	Specific capacitance (mF/cm^2)				
	6AG	6AG-C15	6AG-C30	6AG-C45	6AG-C60
0.1	47.63	90.00	92.13	87.42	112.20
0.25	39.68	65.64	77.00	72.00	86.23
0.5	34.52	59.67	73.30	68.33	82.35
0.75	33.26	57.67	72.33	69.00	82.33
1	31.95	53.00	73.67	68.67	82.12
2.5	27.40	52.00	73.10	68.01	82.10

The specific capacitances of 613AGC-15 to 613AGC-C60 are shown in figure 50 and Table 16. At current density of 0.1 mA/cm^2, the specific capacitances of 613AGC-60 and 613AGC-45 are 239.24 and 234.95 mF/cm^2, respectively. The specific capacitances of 613AGC-30 and 613AGC-15 are 200.85 and 148.00 mF/cm^2, respectively. As shown in figure 50, they can be found that the highest specific capacitance for any current densities can be achieved in the conductive cotton immersed in KMnO$_4$ with citric acid for 60 minutes (613AGC-C60). Therefore, the longer time of immersing in KMnO$_4$ with citric acid provides higher capacitance. This is due to that KOH can be chemical activation of carbon, which creates mesopore and micropore as well as make high specific surface area.
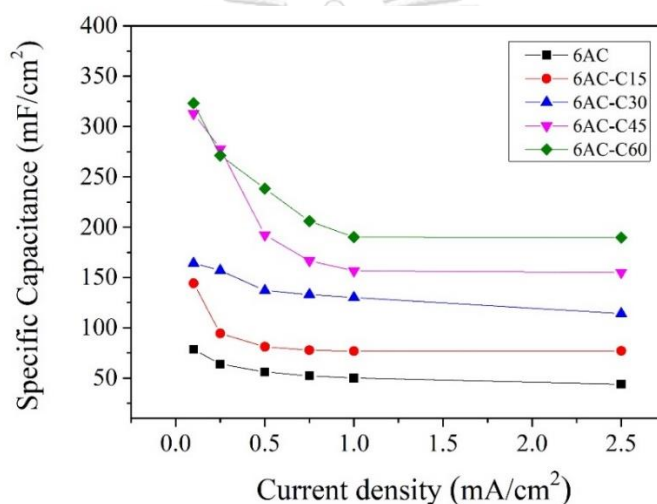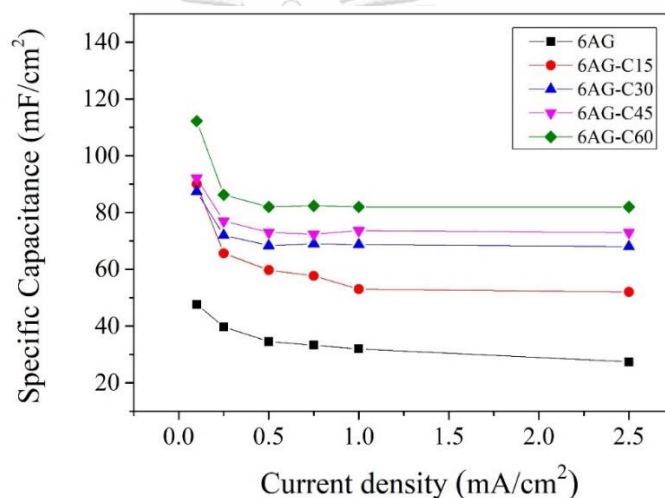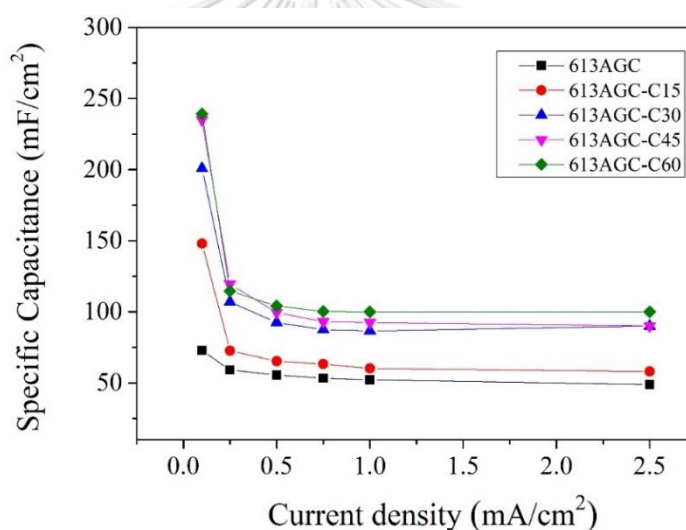

Figure 50 The specific capacitance vs current density of 613AGC-C0 to 613AGC-C60 specimens.

The MnO$_2$ particles cannot be deposited onto the conductive cotton. Thin-film formation by the CBD method is based on the principle of controlled precipitation. The deposition of MnO$_2$ thin films involves several steps such as nucleation, aggregation, coalescence. The MnO$_2$ synthesized by this method used powder. The surface of each conductive cotton (6AC, 6AG or 613AGC) is not rough enough to attach MnO$_2$ particles on the surface.

Table 16 The specific capacitance of 613AGC-C0 to 613AGC-C60 specimens.

Current density (mA/cm^2)	Specific capacitance (mF/cm^2)				
	613AGC	613AGC - C15	613AGC -C30	613AGC -C45	613AGC -C60
0.1	72.91	148.00	200.85	234.95	239.24
0.25	59.05	72.60	200.85	119.95	114.49
0.5	55.60	65.31	107.02	99.50	104.12
0.75	53.36	63.19	92.5	93.00	100.20
1	52.21	60.25	87.50	92.50	100.12
2.5	48.83	58.02	86.50	90.12	100.02

To compare specific capacitance and immersing time of 6AC via KMnO$_4$ with the citric acid solution, the specific capacitance increases with adding more immersing time because KOH can be chemical activation of carbon, which creates mesopores and micropores as well as make high specific surface area (SSA) and high specific capacitance. The KOH activation mechanism can be explained in the assumption as following [25]:

(a) The redox reactions between different potassium compounds as chemical activating carbon reagents, as shown in equations (10-12) called chemical activation, etch the carbon structure. This is responsible for generating the pore network;

$$6KOH + 2C \longrightarrow 2K + 3H_2 + 2K_2CO_3 \quad (10)$$
$$K_2CO_3 + 2C \longrightarrow 2K + 3CO \quad (11)$$
$$C + K_2O \longrightarrow 2K + 3CO \quad (12)$$
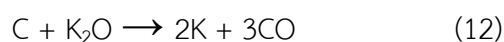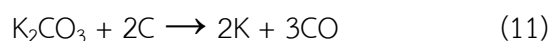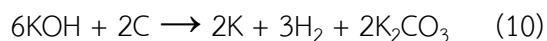
(b) the formation of H$_2$O (equation 13) and CO$_2$ (equations 14 and 15) in the activation system positively contributes to the further production of the porosity through the gasification of carbon, namely physical:

$$2KOH + 2C \longrightarrow 2K_2O + H_2O \qquad (13)$$

$$CO + H_2O \longrightarrow CO_2 + H_2 \qquad (14)$$

$$K_2CO_3 + 2C \longrightarrow 2K + 3CO \qquad (15)$$
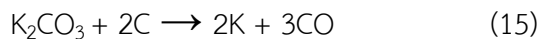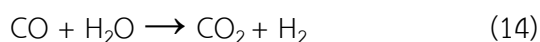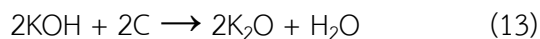
(c) The expansion of the carbon lattices is occurred by the as-prepared metallic K (equations 13-15), efficiently intercalating into the carbon lattices of the carbon matrix during the activation. The expanded carbon lattices cannot return to their previous nonporous structure and thus the high microporosity that is necessary for large specific surface area and micropore volume is created after the removal of the intercalated metallic K and other K compounds by washing [25].
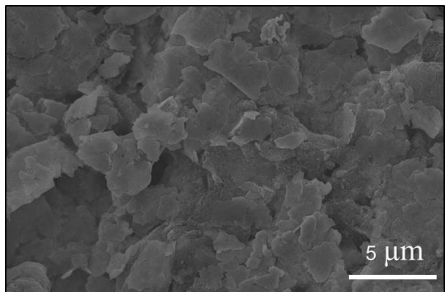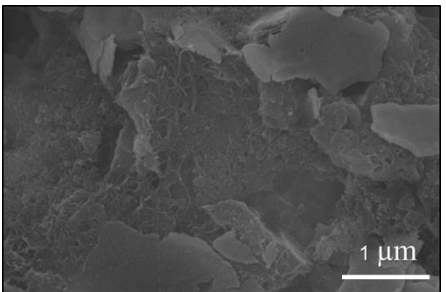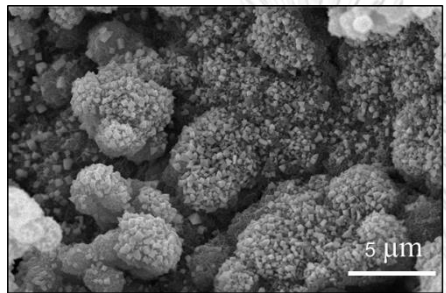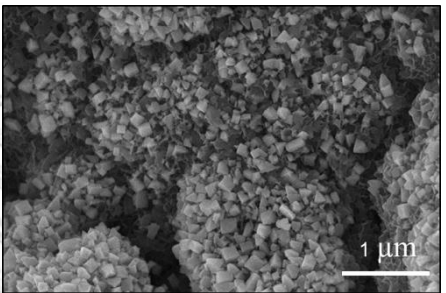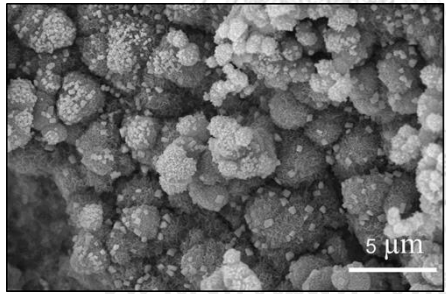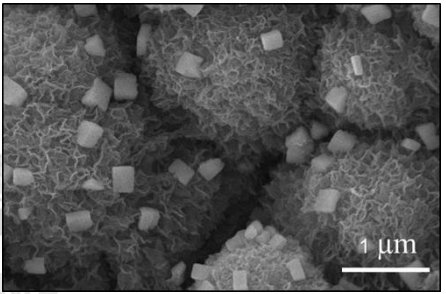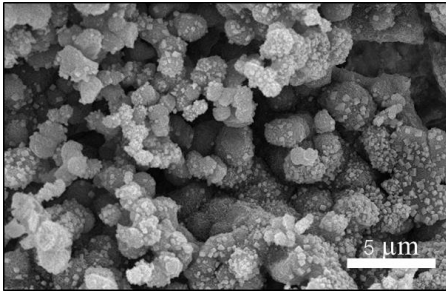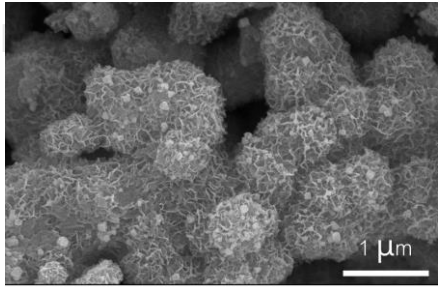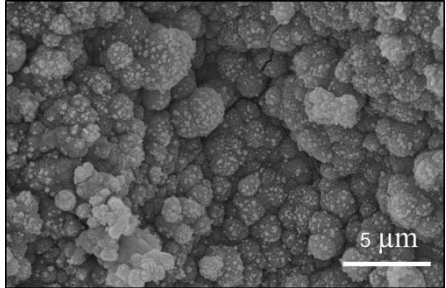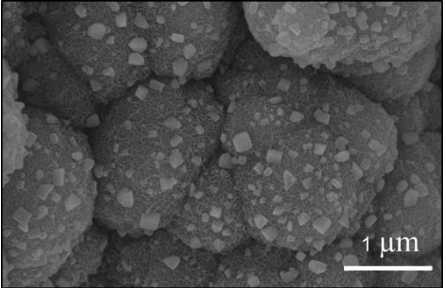
4.3.2 Conductive cotton with MnO_2 electrodes: $KMnO_4$ with H_2SO_4 solution

When sulfuric acid (H_2SO_4) is added in $KMnO_4$, MnO_2 powders is produced by the chemical reaction as shown in equation 16. The microstructure of MnO_2 can be seen in table 17.

$$4KMnO_4 + 3C + 2H_2SO_4 \longrightarrow 4MnO_2 + 3CO_2 + 2K_2SO_4 + 2H_2O \qquad (16)$$
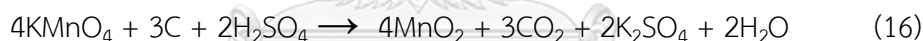
The conductive cotton (6AC) immersed in $KMnO_4$ with the sulfuric acid solution is shown in Figure 51. The black area on the cotton (coating area) is investigated for the morphology, chemical composition and compound by SEM and XRD. SEM images at low magnification (x500) of specimens 6AC-S15 to 6AC-S60 in Table 17 show MnO_2 in cubic and flower-like shape covering on the silver plate. The shape of MnO_2 in specimen 6AC-S60 is less cuboidal than that of specimen 6AC-S15.

Table 17 SEM images of conductive cottons after immersing in $KMnO_4$ with the sulfuric acid solution.

	X 500	X 10,000
6AC		
6AC-S15		
6AC-S30		
6AC-S45		
6AC-S60		
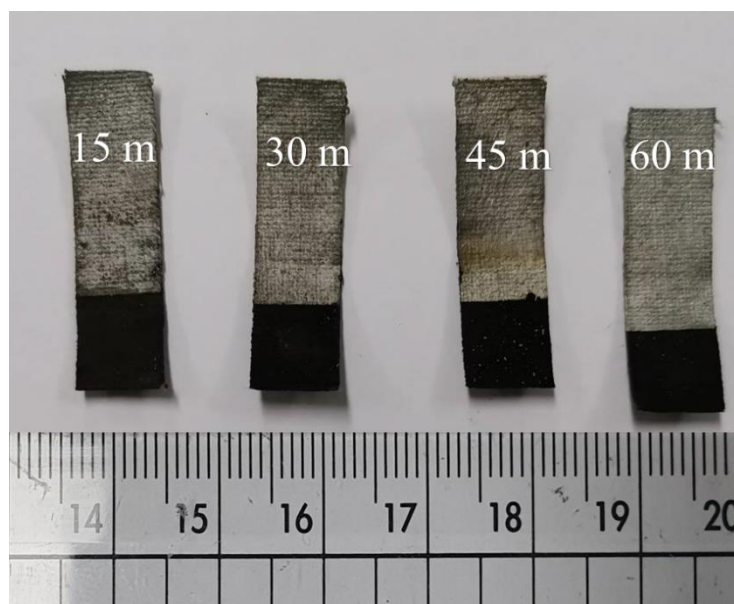
Figure 51 Conductive cottons after immersing in $KMnO_4$ with sulfuric acid for 15, 30, 45 and 60 minutes (dimension of coating area is 1x1 cm^2 (black color))
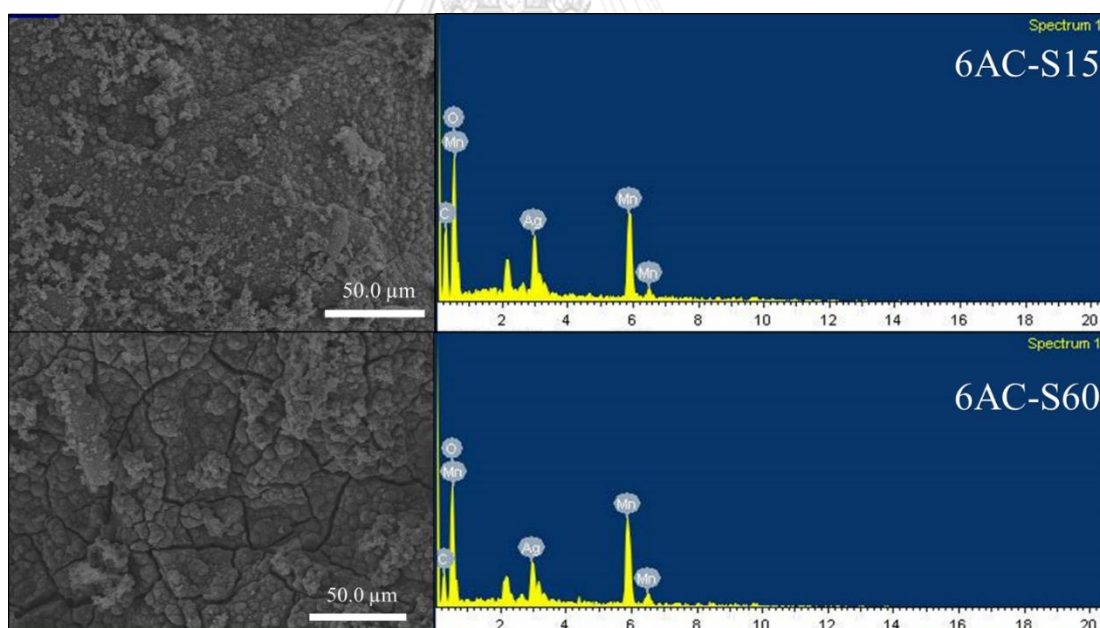
Figure 52 SEM and EDS images of 6AC-S15 (Top) and 6AC-S60 (Bottom)

Figure 52 shows the SEM images and the element for the carbon (C), oxygen (O), silver (Ag) and Manganese (Mn) sources appearing on the conductive cotton.

Chemical composition on the conductive layer of 6AC-S15 is 14.33 wt.% C, 30.79 wt.% O, 38.91 wt.% Mn and 15.98 wt.% Ag while 6AC-S60 is 8.66 wt.% C, 27.01 wt.% O, 48.70 wt.% Mn, and 15.64 wt.% Ag (see Table 18). EDS results show and confirm that MnO_2 powder synthesized in this solution can be deposited onto the cotton.

Table 18 EDS elements of 6AC-S15 and 6AC-S60.

Element	6AC-S15	6AC-S60
	Weight%	Weight%
C K	14.33	8.66
O K	30.79	27.01
Mn K	38.91	48.70
Ag L	15.98	15.64
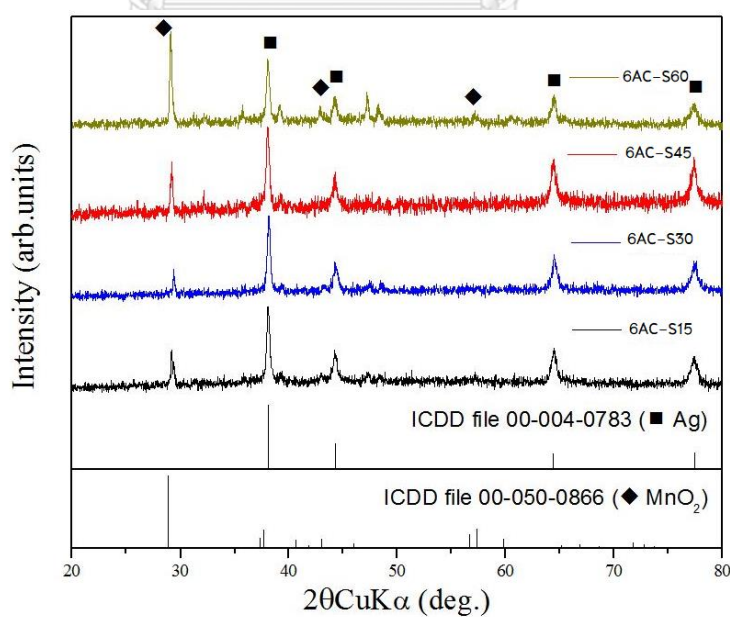
Figure 53 XRD patterns of 6AC-S15 to 6AC-S60 specimens.

The X-ray diffraction (XRD) analysis, which is performed to confirm the crystal structure of 6AC-S15 to 6AC-S60 final products is present in Figure 53. The XRD peak at the 2θ values of 38.166°, 44.277°, 64.426° and 77.472° corresponding to the (1 1 1),(2 0 0),(2 2 0) and (3 1 1) crystal planes of silver are matched with the reported values from the Joint committee on Powder Diffraction Standards card (JCPDS card no.44-0141). The XRD peak at the 2θ values of 28.851°, 56.629 °, 57.361° and 59.767° of Manganese dioxide (JCPDS card no.50-0866) are found on the 6AC-S15 to 6AC-S60. As shown in figure 53, when they are enhanced the immersing time continuously, they can be found that the intensity of MnO_2 peaks are obtained with higher values.
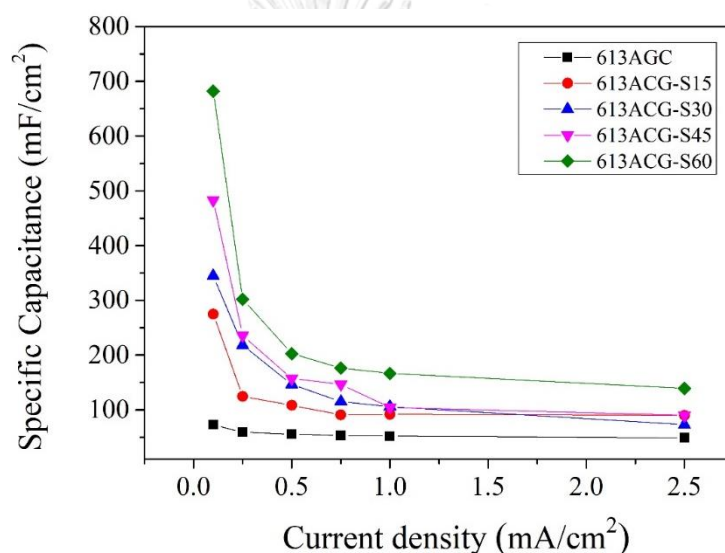
Figure 54 Specific capacitance vs current density of 613AGC-S0 to 613AGC-S60 specimens.

From Figure 54, the specific capacitance is increased by adding more deposition time. Specific capacitance is increased from 274 to 682 mF/cm² at 0.1 mA/cm².However, the specific capacitance is decreased with higher current density (at each sample). Considering with the same current density, the specific capacitance of specimen 613ACG-S15 is lower than that of specimen 613ACG-S60. Therefore, the longer time of immersing in $KMnO_4$ with sulfuric acid provides higher capacitance. This is due to that MnO_2 can be more deposit on the surface that make higher specific capacitance. However, the specific capacitances of all specimens in

the 613AGC group is decreased with increasing current density due to an increase of inner resistance.

Figure 55 shows the specific capacitances of specimens 6AG-S15 to 6AG-S60. The specific capacitance increase when increasing the current density.
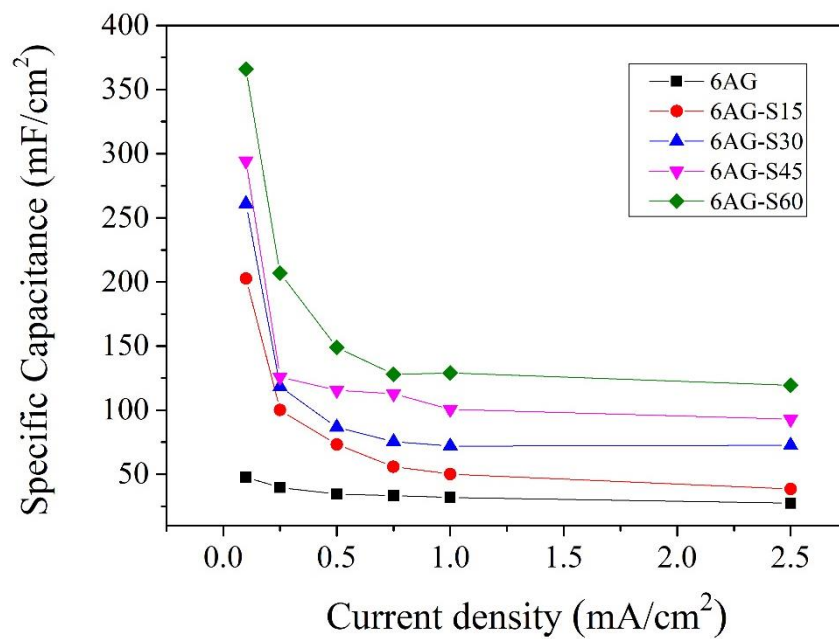
Figure 55 Specific capacitance vs Current density of 6AG-S150 to 6AG-S60
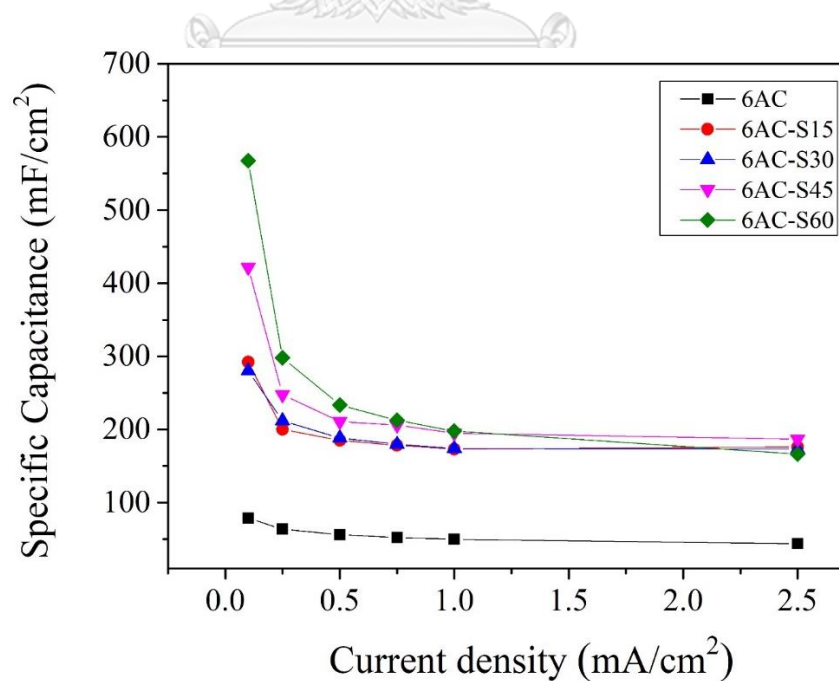
Figure 56 Specific capacitance vs Current density of 6AC-S15 to 6AC-S60 and 6AG-S150 to 6AG-S60

Conductive cottons (consists of carbon nanotube, textile ink and silver powder) are immersed in KMnO$_4$ with sulfuric acid at 15 – 60 minutes. In the result, the higher soaking time does not change specific capacitance value (in high current density) that might be high current density. They do not more time to redox reaction and the redox reaction does not complete to create. The specific capacitance of 6AC-S0 to 6AC-S60 are not different.

Pseudocapacitive (Faradic) reactions are charge storage mechanisms for manganese oxides that reactions occurring on the surface and in the bulk of the electrode. the surface adsorption of electrolyte cations (K+) involves the surface Faradaic reaction on the manganese oxide [27] according to equation 17.
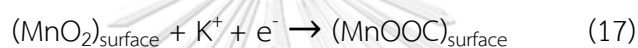
$$(MnO_2)_{surface} + K^+ + e^- \rightarrow (MnOOC)_{surface} \qquad (17)$$

The bulk Faradaic reaction depends on the intercalation or deintercalation of electrolyte cations in the bulk of the manganese oxide to equation 18

$$MnO_2 + K^+ + e^- \rightarrow MnOOC \qquad (18)$$

The adjustment traced inactive materials mainly concerns high reversible capacitance, structural flexibility with stability, fast cation generating under high charge-discharge rates and natural amicability. As a progress metal component, manganese can exist as an assortment of stable oxides.
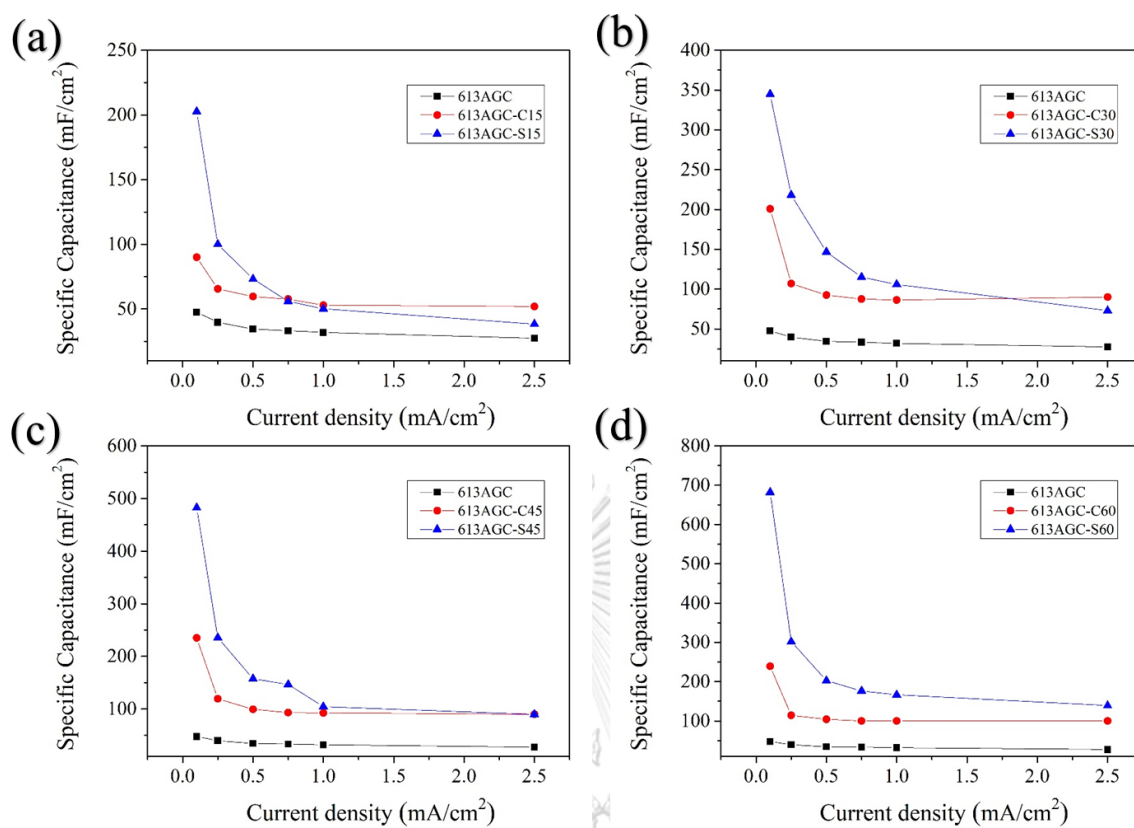
Figure 57 The specific capacitance of conductive cotton after immersing in KMnO$_4$+citric (C-immersing time) and KMnO$_4$ with sulfuric acid (S-immersing time) solutions.

Figure 57 shows the conductive cottons after immersing in KMnO$_4$ with H$_2$SO$_4$ solution (Blue line), which has higher specific capacitance than that of conductive cotton immersed in KMnO$_4$ with citric solution (Red line) because MnO$_2$ synthesized from KMnO$_4$+H$_2$SO$_4$ solution can be deposited onto the conductive cotton surface by a redox reaction. In contrast, the electrical double layer mechanism occurred when the conductive cotton is immersed in KMnO$_4$ with a citric solution.
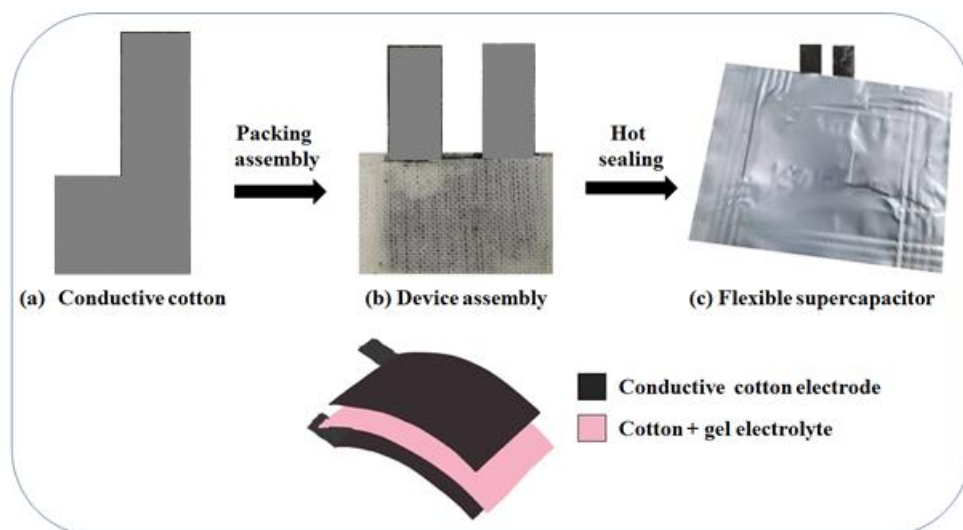
Figure 58 Device assembly of the flexible supercapacitor using the conductive-based cotton textile electrodes.

The CCE electrodes are cut and designed for the assembly of a flexible supercapacitor device as shown in Figure 58 a). Device assembly by 2 conductive cottons and cotton with PVA-KOH gel electrolyte for an optimized concentration of PVA-KOH solid gel electrolyte is performed in this study according to our earlier investigations. The areal specific capacitances obtained at different current densities of the device are shown in Figure 58 b) and Figure 58 c).

Only 6AC is the flexible supercapacitator which can be assembled because there is a leakage problem in the other products. This causes electrolyte to evaporate and dry out making it impossible to measure the voltage.

Flexible supercapacitor is fabricated by this method. Figure 58 the performance of the fabricated flexible device is investigated, the specific areal capacitance values of 677.12, 282.75, 298.89, 288.75, and 319.17 mF/cm^2 are obtained at the rate of 0.0125, 0.05, 0.0625, 0.125 and 0.1875 mA/cm^2, respectively. Moreover, the flexibility of the fabricated supercapacitor device is examined at different twisted bending angles using the cyclic voltammetry experiments. Figure 58 c) shows the cyclic voltammograms obtained after the bending of the device at different angles of 30°, 45°, 60°, 90° and return to the flat position (0°). It should be

noted that the shapes of all the cyclic voltammetry (CV) curves recorded at various angles are almost similar in pattern and a slight variation in the area under the CV loop. It can be observed due to severe stress caused by the extreme bending of the device. This can affect the inner contact region of the interface between the electrode and electrolyte. The corresponding specific capacitances retention at 0 ^{o}, 30°, 45°, 60° and 90° are found to be 100 %, 97.54 %, 92.54 %, 89.19 % and 88.16 %, respectively and retained the value of 99.62% once the bending is returned to 0° from 90° (Figure 58 d)), indicating excellent flexibility of the device is attained even at different twisting angles. This can fulfill the major requirements for the mechanical deformation of the wearable electronics. Furthermore, the cyclic stability of the device is characterized using cyclic voltammetry at a fast scan rate of 100 mV/s (Figure 58 e), which showed outstanding cyclic stability (> 95%) for the first 1000 CV cycles followed by a slightly decreased tendency of the capacitance retention. It is observed that the overall specific capacitance retention value was found to be ~ 80 % for over 3,000 cycles. It could be also observed that the shapes of the CV curves recorded at the initial and final cycles after long-term stability test (Figure 58 f)) display no significant changes indicating the extraordinary cyclic stability of the flexible devices using the conductive cotton electrodes. These results demonstrate that the fabricated flexible supercapacitor device assembled with the optimized electrode composition of the 6AC-CCE specimens shows excellent specific capacitance retention and exceptional cyclic stability even after the being twisted at different bending angles. This can lead to its potential practical applications in portable electronics.
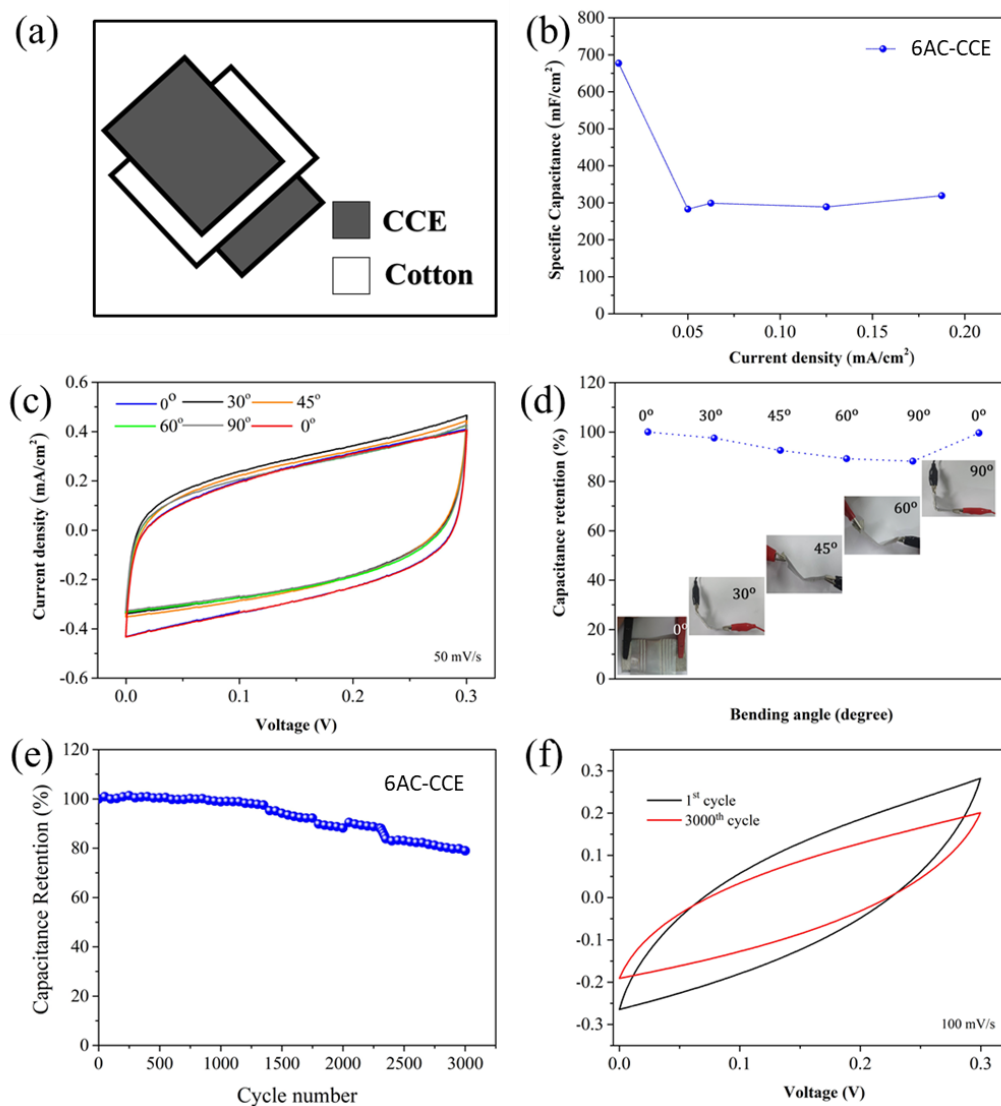
Figure 59 (a) Schematic diagram of the flexible supercapacitor assembly, (b) The specific areal capacitance of the flexible device fabricated using two symmetric electrodes (6AC-CCE) obtained at different current densities, (c) CVs of the flexible device recorded at different bending angles of 0°, 30°, 45°, 60° and 90° and recovered to 0°, (d) Capacitance retention at different bending angles (inset images show the digital photographs taken at different bending angles), (e) Cyclic stability of the flexible device for over 3000 CV cycles and (f) CVs of the 1st and after 3000th cycle (100 mV/s).

Chapter 5

Conclusions

In summary, the conductive cotton based textile electrodes are successfully fabricated using the coating ingredients of silver powder, textile ink and different carbon nanomaterials such as CNTs and graphene as the active components through the screen-printing method. The electrodes prepared with the CNTs' sources show an excellent electrical conductivity, improved electrochemical performance, better rate ability and stability in a strong alkaline electrolyte (6M KOH). The MnO_2 can be deposited after immersing conductive cotton on $KMnO_4$ with H_2SO_4. The specific capacitance shows a higher specific capacitance than those of specimens without MnO_2. Moreover, an asymmetric solid-state flexible supercapacitor device was successfully fabricated with the high-performance electrodes using the PVA-KOH gel electrolyte. The highest areal specific capacitance of 677.12 mF/cm^2 at 0.0125 mA/cm^2 was achieved for the device having suitable electrode composition of the 6AC-CCE specimens (60% silver + 40% CNTs), which retains better flexibility under severe mechanical deformation of different bending angles and shows outstanding cyclic stability for over 3,000 CV cycles. These results demonstrate that the high potential of CCE textile electrodes can further be extended into advanced flexible energy storage devices for viable applications. Futhermore, other conclusions are following below:

1. Silver powder has a great effect on electrical conductivity, which can convert non-conductive cotton to conductive electrode. The resistance of screen-printed cotton with textile ink and silver powder reduces to a low value of 13.64 ± 7.47 ohms/cm.

2. Conductive cotton electrode with CNT can be fabricated by screen printing method using conductive ink and CNT powder. With CNT, the resistance was further decreased from 13.64 ± 7.47 ohms/cm to 6.82 ± 3.82 ohms/cm. The conductive cotton electrode with CNT exhibits good supercapacitor performance. The specific capacitance reach to 78.55 mF/cm^2 at 0.1 mA/cm^2

3. Conductive cotton electrode with graphene nanosheet can be fabricated by screen printing method using conductive ink and graphene powder. With graphene, the resistance was further increase from 13.64 ± 7.47 ohms/cm to 378.67 ± 70.44 ohms/cm. The specific capacitance is 37.85 mF/cm^2 at 0.1 mA/cm^2

4. No MnO_2 was detected on the surface of conductive cotton immersed in $KMnO_4$ with citric acid solution. However, specific capacitance is increased with immersing time. The specific capacitance is 323.17 mF/cm^2 at 0.1 mA/cm^2

5. MnO_2 can be deposited on the surface of conductive cotton in the mixture solution of $KMnO_4$ with sulfuric acid (H_2SO_4). The specific capacitance is increased with immersing time because of high specific capacitance of MnO_2. The specific capacitance reaches to 682.00 mF/cm^2 at 0.1 mA/cm^2

Limitation and suggestion.

1. Adding more screen-printing materials mixed with carbon such as activated carbon and varying their chemical compositions to study and develop the conductive cotton electrode [35] with higher efficiency.

2. The addition of MnO_2 results in higher areal specific capacitance but leads to higher the weight of conductive cotton. Therefore, this means cannot measure the true weight of MnO_2. The weight of MnO_2 would affect specific capacitance values if a higher concentration of MnO_2 provides higher resistance and lower specific capacitance.

3. Assembly of flexible supercapacitors still has some problems. To assemble a cell, heat is required. The workpiece may be damaged, and the packing may be leaked resulting in some electrolyte scattered. The increasing of specific capacitance can be achieved by encapsulation efficiency.

REFERENCES

1. L.Jiří, Supercapacitors: Properties and applications. Journal of Energy Storage, 2018. 17: p. 224-227.

2. S.Patrice, Materials for electrochemical capacitors. Nature Materials, 2008. 7: p. 845-854.

3. GoGotS, P.S.a.Y., Materials for electrochemical capacitors. nature materials, 2008. 7: p. 845.

4. Y.Peihua, Flexible solid-state electrochemical supercapacitors. Nano Energy, 2016. 8: p. 274-290.

5. Dong, L., et al., Flexible electrodes and supercapacitors for wearable energy storage: a review by category. Journal of Materials Chemistry A, 2016. 4(13): p. 4659-4685.

6. Godfrey, A., et al., From A to Z: Wearable technology explained. Maturitas, 2018. 113: p. 40-47.

7. Jones, D.C., The role of wearable electronics in meeting the needs of the active ageing population, in Textile-Led Design for the Active Ageing Population. 2015. p. 173-183.

8. Rodrigues, J.J.P.C., et al., Enabling Technologies for the Internet of Health Things. IEEE Access, 2018. 6: p. 13129-13141.

9. Suryaprabha, T. and M.G. Sethuraman, Design of electrically conductive superhydrophobic antibacterial cotton fabric through hierarchical architecture using bimetallic deposition. Journal of Alloys and Compounds, 2017. 724: p. 240-248.

10. Liu, Z., et al., Advances in Flexible and Wearable Energy-Storage Textiles. Small Methods, 2018. 2(11).

11. Liu, W.-w., et al., Flexible and conductive nanocomposite electrode based on graphene sheets and cotton cloth for supercapacitor. Journal of Materials Chemistry, 2012. 22(33).

12. González, A., et al., Review on supercapacitors: Technologies and materials. Renewable and Sustainable Energy Reviews, 2016. 58: p. 1189-1206.

13.   Simon, P. and Y. Gogotsi, Materials for electrochemical capacitors. Nature
       Materials, 2008. 7(11): p. 845-854.

14.   Jost, K., et al., Knitted and screen printed carbon-fiber supercapacitors for
       applications in wearable electronics. Energy & Environmental Science, 2013. 6(9):
       p. 2698-2705.

15.   Bello, A., et al., Silver nanoparticles decorated on a three-dimensional graphene
       scaffold for electrochemical applications. Journal of Physics and Chemistry of
       Solids, 2014. 75(1): p. 109-114.

16.   Wahid, M., et al., Enhanced Capacitance Retention in a Supercapacitor Made of
       Carbon from Sugarcane Bagasse by Hydrothermal Pretreatment. Energy & Fuels,
       2014. 28(6): p. 4233-4240.

17.   Ferrero, G.A., M. Sevilla, and A.B. Fuertes, Free-standing hybrid films based on
       graphene and porous carbon particles for flexible supercapacitors. Sustainable
       Energy & Fuels, 2017. 1(1): p. 127-137.

18.   Bordjiba, T. and D. Bélanger, Direct Redox Deposition of Manganese Oxide on
       Multiscaled Carbon Nanotube/Microfiber Carbon Electrode for Electrochemical
       Capacitor. Journal of The Electrochemical Society, 2009. 156(5): p. A378.

19.   Du, H., et al., Electric double-layer transistors: a review of recent progress.
       Journal of Materials Science, 2015. 50(17): p. 5641-5673.

20.   Huang, M., et al., MnO2-based nanostructures for high-performance
       supercapacitors. Journal of Materials Chemistry A, 2015. 3(43): p. 21380-21423.

21.   Fu, Y., et al., Fiber supercapacitors utilizing pen ink for flexible/wearable energy
       storage. Adv Mater, 2012. 24(42): p. 5713-8.

22.   Viet Thong Le Heetae Kim, A.G., Jaesu Kim, Jian Chang, Quoc An Vu, Duy Tho
       Pham, Ju-Hyuck Lee, Sang-Woo Kim, and Young Hee Lee, Coaxial Fiber
       Supercapacitor Using All-Carbon Material Electrodes. 2013. 7(7): p. 5940–5947.

23.   Zhang, C., et al., A simple method of fabricating nickel-coated cotton fabrics for
       wearable strain sensor. Cellulose, 2018. 25(8): p. 4859-4870.

24.   Jiang, S.Q., et al., Chemical Silver Plating on Cotton and Polyester Fabrics and its
       Application on Fabric Design. Textile Research Journal, 2016. 76(1): p. 57-65.

25.   Wang, J. and S. Kaskel, KOH activation of carbon-based materials for energy

storage. Journal of Materials Chemistry, 2012. 22(45).

26.   Hu, L., et al., Stretchable, porous, and conductive energy textiles. Nano Lett, 2010. 10(2): p. 708-14.

27.   Weifeng Wei, X.C., Weixing Chena and Douglas G. Ivey, Manganese oxide-based materials as electrochemical supercapacitor electrodes. Chem Soc Rev, 2011. 40: p. 1697-1721.

28.   Chodankar, N.R., et al., Flexible all-solid-state MnO2 thin films based symmetric supercapacitors. Electrochimica Acta, 2015. 165: p. 338-347.

29.   Chen, Y., et al., One-pot synthesis of MnO2/graphene/carbon nanotube hybrid by chemical method. Carbon, 2011. 49(13): p. 4434-4442.

30.   Bélanger, T.B.a.D., Direct Redox Deposition of Manganese Oxide on Multiscaled Carbon Nanotube/Microfiber Carbon Electrode for Electrochemical Capacitor. Journal of The Electrochemical Society, 2009. 156: p. 378-384.

31.   Liu, L., Z. Niu, and J. Chen, Flexible supercapacitors based on carbon nanotubes. Chinese Chemical Letters, 2018. 29(4): p. 571-581.

32.   Ke, Q. and J. Wang, Graphene-based materials for supercapacitor electrodes – A review. Journal of Materiomics, 2016. 2(1): p. 37-54.

33.   Shao, Y., et al., Graphene-based materials for flexible supercapacitors. Chem Soc Rev, 2015. 44(11): p. 3639-65.

34.   Li, J. and M. Östling, Prevention of Graphene Restacking for Performance Boost of Supercapacitors—A Review. Crystals, 2013. 3(1): p. 163-190.

35.   Keawploy, N., et al., Eco-Friendly Conductive Cotton-Based Textile Electrodes Using Silver- and Carbon-Coated Fabrics for Advanced Flexible Supercapacitors. Energy & Fuels, 2020. 34(7): p. 8977-8986.

36.   Keawploy, N., et al, Screen printed textile electrodes using graphene and carbon nanotubes with silver for flexible supercapacitor applications. JMMM. **xx**(xx): p. xxx.

VITA

NAME   Norawich Keawploy

DATE OF BIRTH   4 November 1993

PLACE OF BIRTH   Nonthaburi